ISSN 0869-5911, Petrology, 2021, Vol. 29, No. 2, pp. 148–174. © Pleiades Publishing, Ltd., 2021.
Russian Text © The Author(s), 2021, published in Petrologiya, 2021, Vol. 29, No. 3, pp. 309–336.

Neoarchean Granitoids of the Hautavaara Structure, Karelia: Heterogeneous Lithosphere Melting in an Accretionary Orogen

A. V. Dmitrieva[a, *], F. A. Gordon[b, **], E. N. Lepekhina[c], and N. Yu. Zagornaya[b]

[a] *Institute of Geology, Karelian Research Center, Russian Academy of Sciences, Petrozavodsk, 185910 Russia*
[b] *Institute of Precambrian Geology and Geochronology, Russian Academy of Sciences, St. Petersburg, 199034 Russia*
[c] *Russian Geological Research Institute (VSEGEI), St. Petersburg, 199106, Russia*
**e-mail: dmitrievaa-v@yandex.ru*
***e-mail: fany.gordon@yandex.ru*

Received January 9, 2020; revised September 1, 2020; accepted October 7, 2020

Abstract—The paper presents newly acquired isotope-geochemical and U–Pb isotope zircon dating (SHRIMP) results on four posttectonic granitoid massifs in the southeastern part of the Karelian Granite–Greenstone Province (GGP) in the Fennoscandian Shield. The massifs are located near the Hautavaara Structure, in the southeastern part of the Mesoarchean (3.05–2.85 Ga) Vedlozero–Segozero Greenstone Belt, which is confined to the western margin of the Vodlozero crustal block with a Paleoarchean ($T_{Nd}DM$ > 3.2 Ga) prehistory. All four massifs (Hautavaara, Chalka, Shuya, and Nyalmozero) were shown to have similar structural–tectonic settings, were emplaced nearly simultaneously (at 2745–2740 Ma), and display variations in the rock compositions that were predetermined by differences in the composition of the magma sources and the conditions of their derivation. The Hautavaara Massif in the central part of the structure and the Chalka Massif on its western margin are made up of moderately alkaline high-Mg granitoids (sanukitoids), whose initial diorite melts were derived by melting the lithospheric mantle metasomatized in an active-margin setting at 3.00–2.90 Ga. The Shuya granodiorites and Nyalmozero leucogranites, which are confined to the eastern flank of the structure, yield highly fractionated HREE patterns (Dy_n/Yb_n = 3.5 to 5.14), negative $\varepsilon_{Nd}T$ = –0.9 to –2.8, and were produced by melting a Mesoarchean crustal source at various depths. This source was similar to the 3.05- to 2.90-Ga felsic volcanics in the Hautavaara Structure. The Shuya granodiorites contain elevated Cr and Ni concentrations, suggesting that the melts were generated in the crust with the involvement of mafic magma, which was likely coeval with the primitive sanukitoids. The melting of the continental lithosphere at mantle and crustal levels in the Karelian GGP in the latest Neoarchean are thought to have occurred in an extensional environment during collapse of the collisional orogen, in accordance with the model (Laurent et al., 2014).

Keywords: Karelian granite–greenstone region, Neoarchean sanukitoids and granites, geochemistry, U–Pb geochronology, petrology

DOI: 10.1134/S086959112102003X

INTRODUCTION

Granite–greenstone provinces (GGP) are the best preserved remnants of the Archean crust and, hence, may provide valuable information on crust-forming processes during various episodes of the Earth's evolution. Similarities in the structures and composition of rocks in GGP of different age at various cratons is predetermined by that these belts persistently contain two major tectono-stratigraphic complexes: tonalite–greenstone and granitoid ones. The older tonalite–greenstone complex is made up of volcano-sedimentary sequences of greenstone belts and surrounding tonalite–trondhjemite–granodiorite (TTG) plutons. The younger granitoid complex consists of compositionally variable granitic rocks, which occur at relatively extensive areas within GGP and were emplaced after one or multiple episodes of deformations and metamorphism of the rocks of the tonalite–greenstone complex (Condie, 1981). Although such complexes have long been studied at many cratons, many aspects of their origin and the tectonic setting in which they were formed remain a matter of heated discussions and are still intensely explored. One of such complexes is the Karelian GGP, whose rocks crop out in the southeastern Fennoscandian Shield and are studied for more than one century.

The researchers focus primarily on the origin and tectonics of the rocks of the tonalite–greenstone complex. Greenstone belts have long been thought to be systems of ensialic rifts initiated by a deep-sitting plume, whereas TTG granitic rocks in the surrounding structures were viewed as a remobilized basement

(Rybakov et al., 1981, 1993). In the past decades, TTG–greenstone belts are discussed as accretionary orogens in which complexes of oceanic plateaus, island arcs, and active margin were tectonically combined (Puchtel et al., 1997, 1999; Kozhevnikov, 2000; Bibikova et al., 2003; Svetov, 2005).

Keen interest in the complex of Archean granitic rocks in the Karelian GGP was whetted by that sanukitoids (mildly alkaline magnesian granitic rocks) were found in it (Chekulaev, 1999). These granitoids are widespread in the Karelian GGP, compositionally vary from monzodiorite to monzogranite, and make up single- or polyphase massifs of different size. Regional studies have shown that, although sanukitoid massifs in the eastern Karelian GGP and its western part are similar in composition, the former are older: 2745–2735 and 2720–2700 Ma, respectively (Heilimo et al., 2011 and references therein). Detailed studies of a number of polyphase intrusions made it possible to reproduce the generation parameters of the parental sanukitoid melts and their subsequent differentiation during ascent to upper crustal levels (Samsonov et al., 2004; Lobach-Zhuchenko et al., 2005, 2008). The results of these studies generally lead to a consistent and unambiguous model for the generation of sanukitoids in the Karelian GGP via the melting of metasomatized lithospheric mantle and the subsequent differentiation and contamination of the melts during their ascent to upper crustal levels (Halla, 2005; Kovalenko et al., 2005; Larionova et al., 2007; Lobach-Zhuchenko et al., 2008). Therewith a disputable issue is the tectonic environments in which the melts were derived, which are hypothesized to have been either an island arc, active continental margin, a postsubductional environment, or a plume (Martin et al., 2009; Samsonov et al., 2004; Chekulaev et al., 2018).

Granites and granodiorites of normal alkalinity not related to sanukitoids were studied in the western Karelian GGP by many researchers, and the results of these studies are summarized in (*Rannii ...,* 2005; Höltta et al., 2012; Chekulaev et al., 2020). The data indicate that the granitoids were produced within a brief age interval of 2720–2680 and show broadly variable geochemical and isotopic parameters, which were predetermined by the variations in the P–T–C_{H_2O} melting parameters of the compositionally and isotopically–geochemically heterogeneous crust of the Karelian GGP. It was hypothesized (Chekulaev et al., 2020) that the extensive melting of the crust and the massive generation of the granitic magmas in the latest Archean were induced by a deep-sitting plume. It is worth mentioning that, although the age ranges in which sanukitoids and granites were formed in the western Karelian GGP overlap, aspects of the genetic and/or tectonic relations between these rocks are not discussed.

To evaluate the age and genetic relationships between constituents of the granitoid complex of the Karelian GGP, we have conducted geological–petrographic and isotopic–geochemical studies of rocks, and carried out their U–Pb zircon dating (SHRIMP-II) from four post-tectonic massifs that are made up of rocks of different composition (monzodiorite and monzogranite of the sanukitoid series, tonalite, granodiorite, and leucogranite) and occur within a relatively small area in the Hautavaara Structure in the Vedlozero–Segozero Greenstone Belt.

GEOLOGY OF THE HAUTAVAARA STRUCTURE

The Hautavaara Structure is constrained to the boundary between the Vodlozero and Central Karelian domains of the Baltic Shield and is the southern tip of the Vedlozero–Segozero Greenstone Belt (Fig. 1a). The Vodlozero Domain is a fragment of the ancient continental crust, and its granitoids are rocks of a TTG complex (3.24 and 3.15–3.13 Ga), trondhjemites (2.9 Ga), sanukitoids (2.74–2.73 Ga), and granites (2.70–2.68 Ga) (*Rannii ...,* 2005; Arestova et al., 2015). The Central Karelian Domain consists of younger complexes, including TTG ones (2.78–2.77 Ga), sanukitoids (2.75–2.71 Ga), trondhjemites, and granites (2.72–2.70 Ga) (*Rannii ...,* 2005).

The Hautavaara Structure includes an earlier basalt–andesite–dacite–rhyolite series. The volcanics were dated using zircon from the dacites at 2995 ± 20 Ma (Svetov, 2005 and references therein) and 2945 ± 19 Ma (Ovchinnikova et al., 1994) and using zircon from dacite fragments in the agglomerates at 2944 ± 7.9 Ma (Matrenichev et al., 1990). The island-arc complex is overlain by an allochthonous komatiite–basalt association, whose Sm–Nd isochron age is 3.18–2.92 Ga (Svetov et al., 2006; Svetov and Huhma, 1999). The age of the later andesite–dacite series is 3.0–2.98 Ga (Svetov et al., 2006), and the cutting dacite and rhyolite dikes were dated at approximately 2.85 Ga (Ovchinnikova et al., 1994). The geological sequence of the Hautavaara Structure is topped by basalts and volcano-sedimentary rocks, which crop out in the northeastern part of the structure (Svetov, 2005).

The intrusive rocks of the Hautavaara Structure compose mafic–ultramafic and granitic complexes (Fig. 1b). The ultramafic rocks (serpentinized peridotites, olivinites, and pyroxenites) occur at a number of levels, intrude the Mesoarchean volcanic rocks, and are, in turn, cut by gabbroic rocks. The melanocratic gabbro and conformable tabular intrusions, which are noted for elevated magnetization, are grouped into the Vietukkalampi ferrogabbro complex (Slyusarev et al., 2007), whose gabbro-pegmatite has a U–Pb zircon age of 2914 ± 9 (Nosova et al., 2013). The eastern flank of the structure hosts bodies of the Kainooja gabbro complex, which cut across volcanic rocks of acid–intermediate composition (>2.85 Ga).

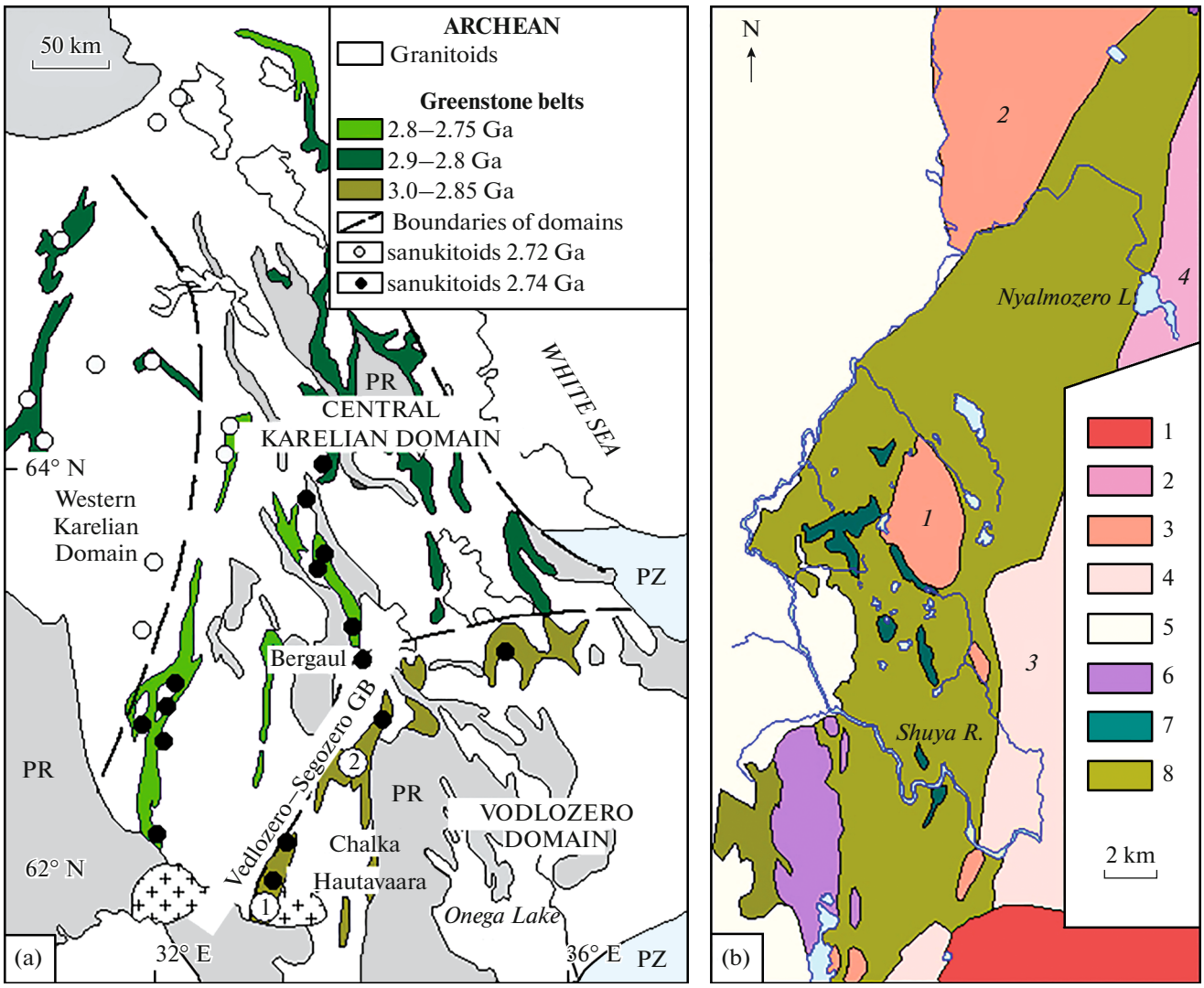

Fig. 1. (a) Schematic location map of the Hautavaara Greenstone Structure (according to Lobach-Zhuchenko et al., 2005; Heilimo et al., 2013) and (b) its schematic geological map (based on materials of the Karelian Geological Expedition, Production Report by V.V. Sivaev and A.F. Goroshko, 1988; *1 : 200000 Geologicheskaya karta SSSR, List* P-36-XV). (a) (1) Hautavaara Structure; (2) Koikara Structure. (b) Rapakivi of the Ulyalega Massif (1.5 Ga); (2) mildly alkaline leucogranite of the Nyalmozero Massif; (3) granitoids of the Hautavaara Complex (2.74 Ma); (4) Shuya granodiorite massif; (5) unclassified granites and granite-gneisses; (6) ultramafic rocks of the Hyursul Complex; (7) ferrogabbro of the Vietukkalampi Complex (2.9 Ga); (8) Meseoarchean volcanic and volcano-sedimentary rocks (3.0–2.85 Ga). Massifs: (*1*) Hautavaara, (*2*) Chalka; (*3*) Shuya; (*4*) Nyalmozero.

Granitic magmatism of the Hautavaara Structure produced TTG gneisses and granitic rocks, some of which are recognized as the Shuya Complex, sanukitoids (Hautavaara Complex), potassic granites (Nyalmozero Complex), and a complex of small intrusions (Virtaoja Complex).

The Shuya Complex has been regarded as a product of TTG magmatism and was correlated with analogous granitoid complexes produced in the Karelian GGP at 2.86–2.85 Ga (Kuleshevich et al., 2009), and the pluton in the eastern flank of the Hautavaara Structure was referred to as the Shuya Massif.

The Hautavaara Complex, which comprises the Hautavaara and Chalka massifs and a number of smaller bodies, cuts the folded and metamorphosed greenstone sequence and ferrogabbro bodies. Based on their geochemical characteristics, the rocks of this complex were classed with the sanukitoid series (Lobach-Zhuchenko et al., 2000, 2005). The U–Pb zircon age (NORDSIM and classic method) of the intrusions is ~2.74 Ga (Bibikova et al., 2005; Ovchinnikova et al., 1994).

The potassic granites of the Nyalmozero Massif in the northeastern part of the Hautavaara Structure are thought to be analogues of the mildly alkaline granites of the final magmatic phase (2.70–2.68 Ga) of the greenstone belts.

The Virtaoja Complex of small intrusions comprises vein bodies of tourmaline–muscovite leucogranites with microcline–plagioclase pegmatites.

The granites of the Ulyalega Massif (~1.54–1.5 Ga) cut across greenstone sequence in the southern part of the structure.

METHODS

Analysis for major oxides was conducted by conventional silicate analysis at the Analytical Center of the Karelian Research Center, Russian Academy of Sciences, in Petrozavodsk. The analyses were accurate to 1–5 relative % at concentrations >0.5 wt % and no worse than 12 relative % at concentrations <0.5 wt %.

Concentrations of trace elements were analyzed by ICP-MS on an X-Series 2 (Thermo Fisher Scientific) quadrupole mass spectrometer at the Center for Collective Use of the Karelian Research Center, Russian Academy of Sciences, by conventional methods (Svetov et al., 2015). The samples were decomposed with acids in an open system. The accuracy of the analyses was controlled by replicate analyses of the BHVO-2, SGD-1A, and SGD-2A certified standard reference samples.

Local U–Pb dating of zircons was conducted by SIMS (SHRIMP-II) at the Center for Isotope Studies of the Karpinsky Russian Geological Research Institute of Geology (VSEGEI) in St. Petersburg by conventional methods (Williams, 1998; Larionov et al., 2004). Epoxy pellets with grains of the zircon and the TEMORA (Black et al., 2003) and 91500 (Wiendenbeck et al., 1995) standards were polished to expose the grains to roughly half of their thicknesses and were sputter coated with ~10 Å layer of 99.999% Au. The inner structures of the zircon grains were examined using optical and electron microscopy. The cathodoluminescence (CL) and back-scattered electron (BSE) images were acquired on a CamScan MX2500 scanning electron microscope. The secondary current was measured using a high-frequency secondary-electron multiplier in a mass-scanning mode. The intensity of the primary beam of negatively charged molecular oxygen ions was ~3 nA, and the craters were ~25 μm in diameter. The raw data were processed with the SQUID v. 1.13 and ISOPLOT/Ex 3.41b softwares (Ludwig, 2001, 2003). The U–Pb ratios were normalized to the value of 0.0668 for the TEMORA zircon standard, which corresponds to a zircon age of 416.75 Ma (Black et al., 2003). The U concentration standard was the 91500 zircon standard with an U concentration of 81.2 ppm (Wiedenbeck et al., 1995). The analytical errors of individual analyses (isotope ratios and age) are reported on an 1σ level, and the errors of the concordant ages are reported on a 2σ level.

The isotope composition of Sm and Nd was analyzed on a Triton T1 multicollector mass spectrometer at the Laboratory of Isotope Geology, Institute of Precambrian Geology and Geochronology, Russian Academy of Sciences, in St. Petersburg, according to the technique described in (Kotov et al., 1995). Concentrations of Sm and Nd were analyzed accurate to ±0.5% (2σ), the $^{147}Sm/^{144}Nd$ and $^{143}Nd/^{144}Nd$ isotope ratios were measured accurate to ±0.5% and ±0.005% (2σ), and the weighted mean $^{143}Nd/^{144}Nd$ ratio of the La Jolla standard was 0.511894 ± 8. The $\varepsilon_{Nd}(T)$ values were calculated using modern values for the chondrite uniform reservoir (CHUR) $^{143}Nd/^{144}Nd = 0.512638$ and $^{147}Sm/^{144}Nd = 0.1967$ (Jacobsen and Wasserburg, 1984) and the depleted mantle (DM) $^{143}Nd/^{144}Nd = 0.513151$ and $^{147}Sm/^{144}Nd = 0.2136$(Goldstein and Jacobsen, 1988).

GEOLOGY AND PETROGRAPHY OF THE MASSIFS

The ***Hautavaara Massif*** was studied most thoroughly. It is situated in the central part of the Hautavaara Structure, cuts across folded and metamorphosed greenstone sequences, and is meridionally elongate and extends for up to 6 km in this direction. The intrusion has a complicated inner structure and consists of two intrusive phases (Dmitrieva et al., 2016). Phase 1 comprises monzogabbrodiorite and monzodiorite, and its rocks are subordinate in the southern and western inner contact zones of the intrusion (Figs. 2, 3a, 3b). The massif is dominated by rocks of phase 2: granosyenite, and monzogranite (Figs. 3c, 3d), which host fragments of phase-1 rocks.

The U–Pb zircon age of the Hautavaara Massif is 2743 ± 8 Ma for the monzodiorite, 2742 ± 23 Ga for the monzogranite (Bibikova et al., 2005), and 2735 ± 2 Ga for the granosyenite (Stepanova et al., 2014).

The rocks of the Hautavaara intrusion are usually massive. The monzogabbrodiorites are equigranular or porphyritic, with microcline phenocrysts, contain plagioclase (50–55%), K-feldspar (4–5%), hornblende (25–30%), biotite (10–15%), quartz (~3%), titanite (2%), apatite (0.5–1%), ilmenite, and accessory zircon and monazite. The monzodiorites are usually porphyritic rocks owing to feldspar phenocrysts. The rocks contain plagioclase (50–60%), K-feldspar (15–20%), hornblende (10–15%), biotite (15–20%), quartz (~3%), titanite (1–2%), and accessory zircon and monazite.

The quartz monzodiorites are medium-grained massive rocks made up of plagioclase (30–35%), K-feldspar (40–45%), biotite (~8%), quartz (5–10%), and accessory titanite (1–2%), apatite (0.5%), zircon, and more rare allanite. The leucocratic granosyenites and pinkish red monzogranites are medium- to coarse-grained porphyritic massive or patchy rocks. The granosyenites consist of plagioclase (30–35%), K-feldspar (35–45%), quartz (20%), biotite (5–10%), and accessory titanite (1–2%), apatite, zircon, and monazite. The monzogranites contain more K-feld-

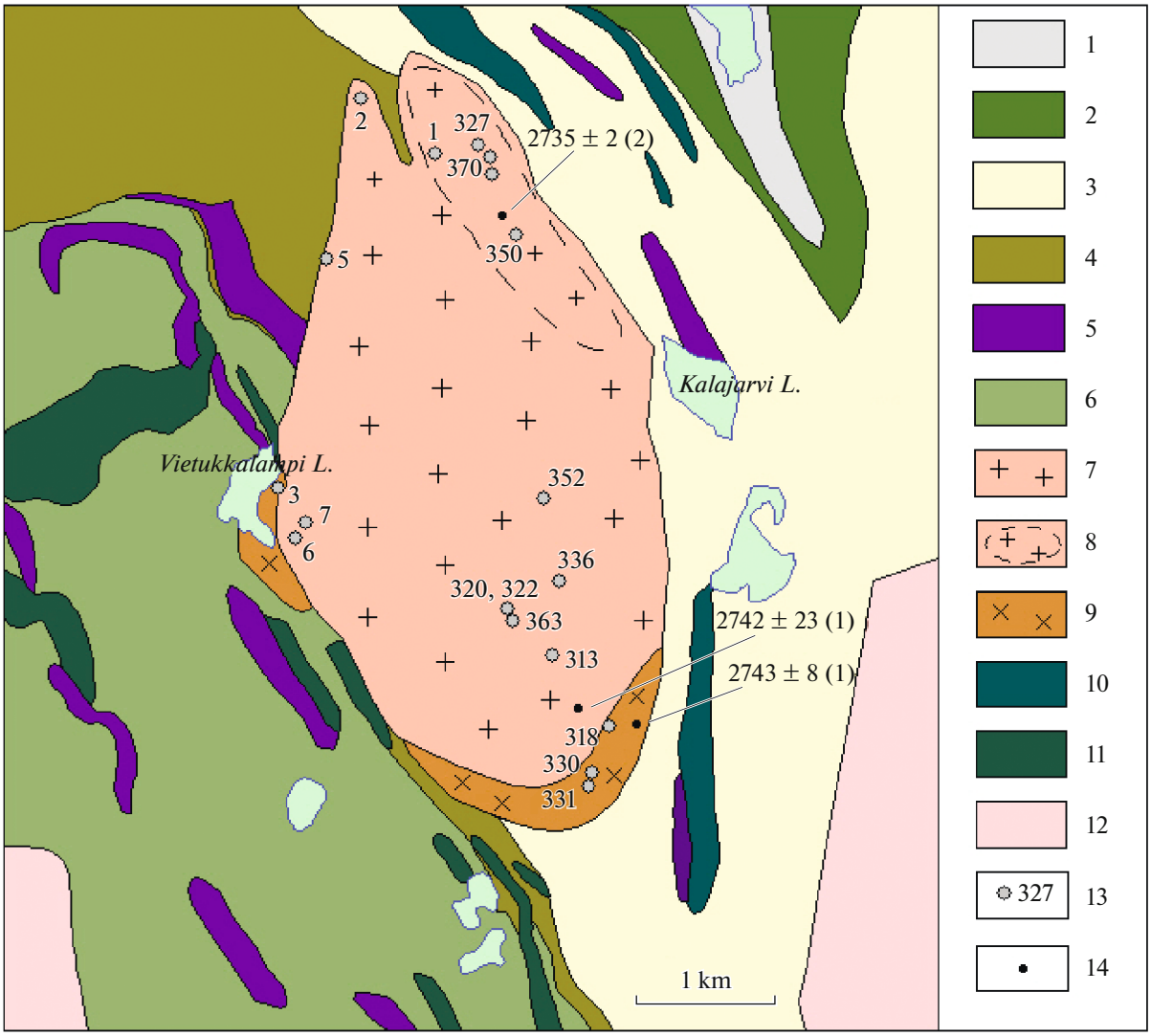

Fig. 2. Schematic geological map of the Hautavaara Massif (based on materials of the Karelian Geological Expedition, Production Report by V.V. Sivaev and A.F. Goroshko, 1988) (1) Tuff and tuff–sedimentary rocks; (2) basalt; (3) andesites–dacite series and related volcano-sedimentary rocks (>2.85 Ga); (4) komatiite–basalt series and related volcano-sedimentary rocks (3.05–2.90 Ga); (5) ultramafic rocks; (6) BADR-series (3.05–2.95 Ga); (7–9) Hautavaara Massif ((7) monzogranite, (8) granosyenite, (9) monzogabbrodiorite and monzodiorite); (10) gabbro of the Kainooja Complex; (11) ferrogabbro of the Vietukkalampi Complex; (12) granitoids of the Shuya Complex; (13) sampling sites; (14) sites of rocks dated by U–Pb methods: (1) (Bibikova et al., 2005), (2) (Stepanova et al., 2014).

spar (40–55%) and quartz (20–25%) but less plagioclase (20–30%), their mafic mineral is biotite (5–10%), and the accessory minerals are titanite (up to 3%), apatite (up to 0.5%), zircon, and monazite.

The ***Chalka Massif*** bounds the greenstone sequence of the Hautavaara Structure in the northwest and cuts the granitoids of structures surrounding it in the west (Fig. 4). The massif is meridionally elongate and, according to geophysical and geological-survey data, is large (approximately 20 km along its major axis). The massif consists of diorites and quartz diorites. The rocks are replaced by epidote in the marginal portion of the massif and are cut by numerous aplite and pegmatite veins. The northern part of the Chalka Massif is overlain by a mantle of glacial drift. The U–Pb zircon age of the massif is 2745 ± 5 Ma (Ovchinnikova et al., 1994).

The Chalka Massif is dominated by mesocratic coarse-grained or porphyritic (with feldspar phenocrysts) biotite–hornblende quartz diorites (Figs. 3e–3g). The rocks consist of plagioclase (60–75%, oligoclase or more rare andesine), K-feldspar (0–5%), quartz (5–12%), hornblende (5–15%), biotite (7–12%), apatite (up to 1%), titanite, and REE-bearing titanite (up to 1–2% REE), zircon, and secondary epidote, Ce-epidote, (3–5% REE), chlorite (1%), carbonates (including those of the bastnaesite–parasite series), and barite. The alterations of the quartz

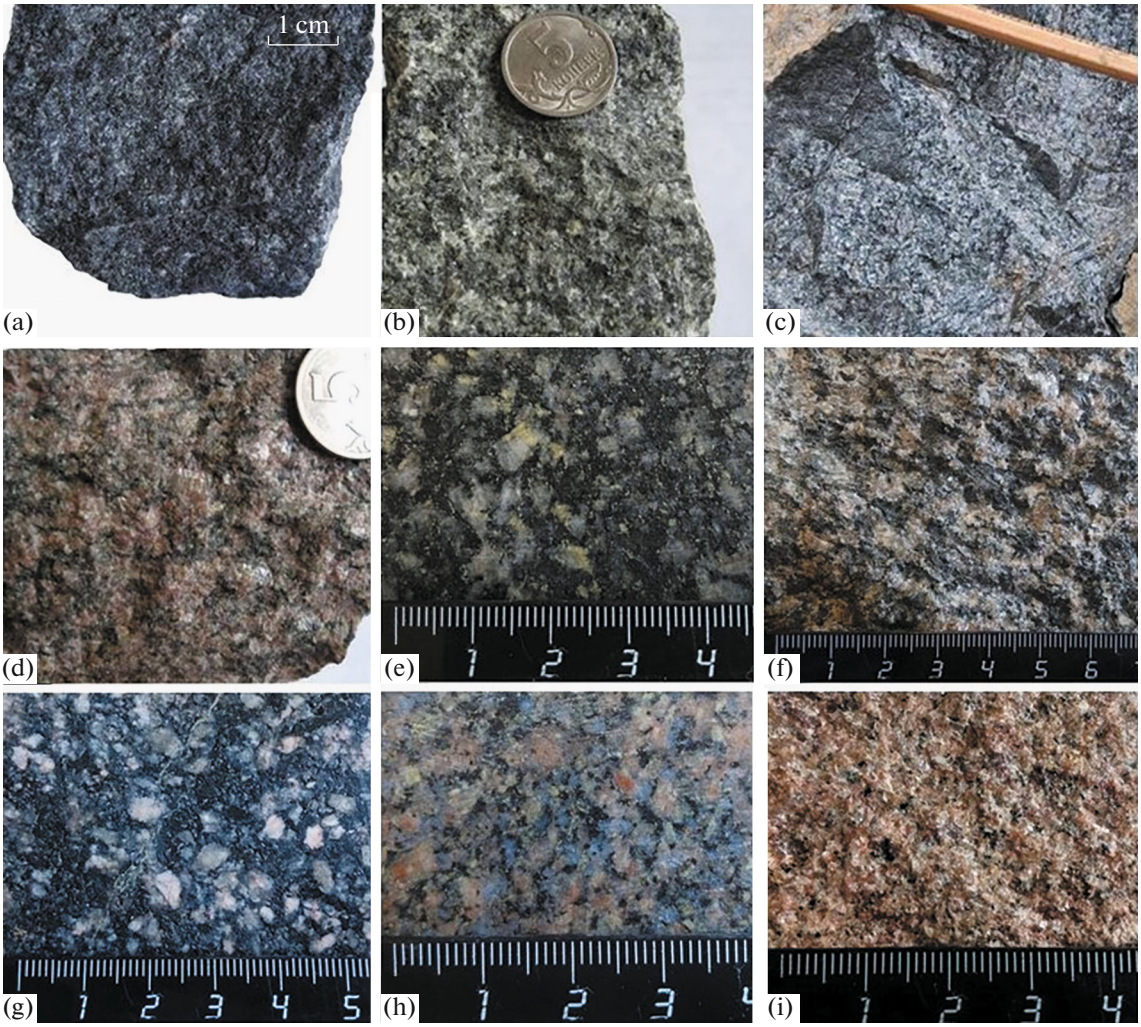

Fig. 3. Rock varieties of granitoid massifs of the Hautavaara Structure. (a–d) Hautavaara Massif ((a) monzogabbrodiorite, sample 3/1, (b) monzodiorite, sample 330, (c) granosyenite, sample 350, (d) monzogranite, sample 363), (e–g) Chalka Massif ((e) epidotized quartz diorite, sample 660, (f) quartz diorite, sample 662, (g) porphyritic quartz diorite, sample 665), (h) Shuya Massif (granodiorite, sample 526), (i) Nyalmozero Massif (monzoleucogranite, sample 678).

diorites involve the extensive replacement of their plagioclase by epidote, which makes the rock greenish, and biotite replacement by chlorite.

The ***Shuya Complex*** comprises (according to geological survey data of the Karelian Geological Expedition) four magmatic phases: (1) diorite; (2) plagiogranite, tonalite, and granodiorite; (3) granite and microcline leucogranite; and (4) veins of microcline pegmatite, which marked the final episode of the magmatism. The granitoids of the Shuya Complex were found in the surroundings of the Hautavaara Structure (Fig. 5). They bound the greenstone sequences in the west and east and are broken by a number of faults of near-meridional and northwestern trend. In the zones of contacts between the granitoids and volcanic rocks and around fault zones, the rocks are affected by cataclasis, mylonitization, and albitization. The Shuya Complex covers a large area but is poorly exposed on the surface, because of which we managed to study only its granodiorite phase in the eastern and southern parts of the structure.

The granodiorites are massive pale reddish coarse-grained rocks and are noted for containing blue quartz (Fig. 3h). They consist of K-feldspar (6–20%), plagioclase (50–60%), quartz (15–20%), biotite (5–6%), and secondary (2–5%), epidote (4–5%), carbonate, and chlorite. The accessory minerals are apatite, titanite (1%), and zircon. The plagioclase is replaced by epidote and sericite, and the biotite is replaced by chlorite. When intensely epidotized and sericitized, the rocks become greenish. Their sheared and cataclased varieties are richer in quartz and biotite. The ore minerals are rutile, pyrite, and galena. The rocks are cut by pyrite-bearing quartz–epidote veinlets.

The ***Nyalmozero Massif*** cuts the volcanic and volcano-sedimentary sequences in the northeastern part

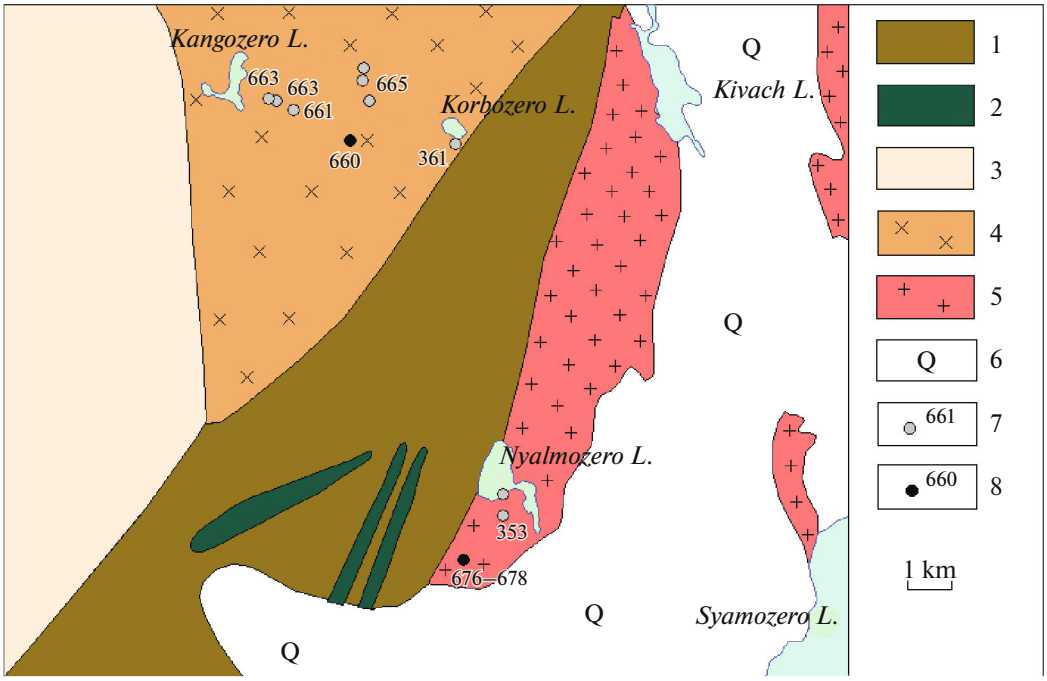

Fig. 4. Schematic geological map of the Chalka and Nyalmozero massifs (modified after *1 : 200000 Geologicheskaya karta SSSR, List P-36-XV*). (1) Volcanic and volcano-sedimentary rocks; (2) metagabbro; (3) unclassified Archean granitoids; (4) diorites of the Chalka Massif; (5) monzoleucogranites of the Nyalmozero Massif; (6) Quaternary rocks; (7) sampling sites; (8) sampling sites for U–Pb dating and sample numbers.

of the Hautavaara greenstone structure. The massif extends nearly meridionally for up to 15 km and is made up of pale pink mildly alkaline leucogranites. Intrusive bodies of similar composition are also found north and east of this massif and may be fragments of a single pluton that is partly overlain by Quaternary rocks (Fig. 4).

The monzogranites are massive fine-grained, sometimes slightly sheared rocks and consist of K-feldspar (25–30%), plagioclase (25–30%, oligoclase or more rare albite), quartz (35–40%), biotite (3–5%), and muscovite (2–3%). The dominant accessory mineral is monazite, and the rocks also contain accessory apatite and zircon. The secondary minerals are epidote (1–3%), sericite, and chlorite. The rocks contain minor amounts of rutile, ilmenite, and galena.

CHEMICAL COMPOSITION OF THE ROCKS

We have most thoroughly studied and sampled the ***Hautavaara Massif*** (Dmitrieva et al., 2016). The composition of its rocks broadly varies, with SiO_2 concentration increasing from 51.98 wt % in the monzogabbrodiorites to 70.5 wt % in the monzogranites and the total of alkalis simultaneously increasing from 6.21 to 9.57 wt % (Table 1, Fig. 6). The rocks belong to the moderately alkaline series, with K_2O dominating over Na_2O ($Na_2O/K_2O < 1$) and possess elevated Mg# = 0.60–0.45, which decreases with increasing SiO_2 and Al_2O_3 concentrations. The phase-2 granosyenites and monzogranites are poorer in FeO*, MgO, CaO, TiO_2, and P_2O_5 than the monzogabbrodiorite and monzodiorite. In Harker diagrams (Fig. 6), the correlations between major-element concentrations and SiO_2 are almost rectilinear (Fig. 6).

The phase-1 monzogabbrodiorite and monzodiorites bear elevated concentrations of P_2O_5 (0.56–0.61 wt %), TiO_2 (0.65–1.03 wt %), and V (128–201 ppm), and these rocks are richer in Cr (163–223 ppm), Ni (49–70 ppm), and Cu (18–118 ppm) than the phase-2 granosyenites and monzogranites (Cr 20–68, Ni 10–37 and Cu 6–29 ppm) (Figs. 6, 7). The rocks of phase 1 are enriched in Zr with an increase in the SiO_2 concentration, whereas Zr concentration in the phase-2 rocks, conversely, decreases with increasing SiO_2 concentration (Fig. 7). The Ba and Sr concentrations decrease from the mafic to acid rocks, whereas the Rb concentration increases. The maximum Ba concentration in the monzogabbrodiorites and monzodiorites is 2054 ppm, and those in the granosyenites and monzogranites are 1081 ppm.

The rocks of the Hautavaara Massif typically have fractionated REE patterns, $(La/Yb)_n = 14–21$, and the total REE concentrations decrease from 346 to 128 ppm with increasing silicity (Fig. 8).

The ***Chalka Massif*** was sampled in its southern part, and was traversed from its eastern inner contact zone in the Korbozero Lake area westward to Kangoz-

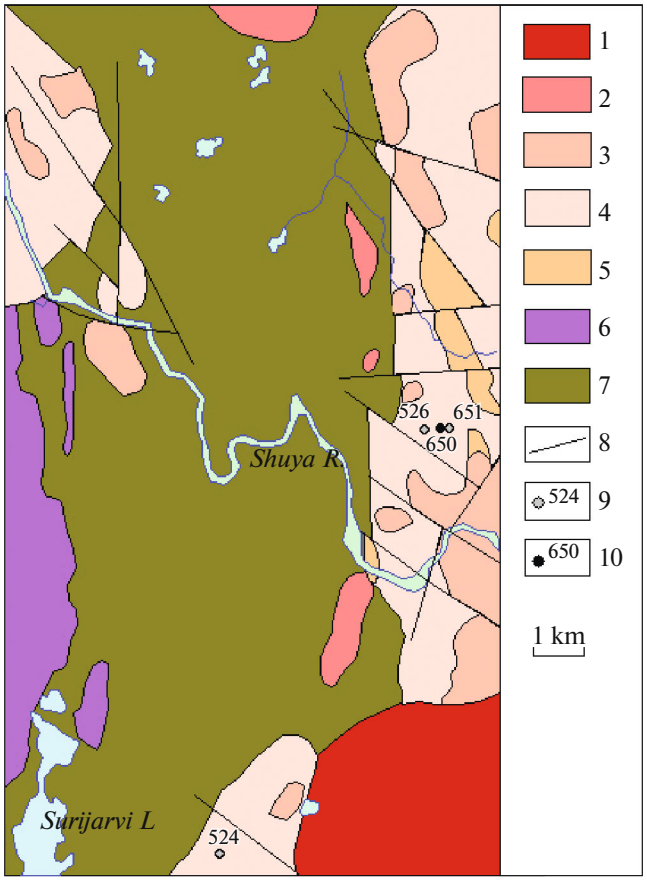

Fig. 5. Schematic geological map of the Shuya Complex (based on materials of the Karelian Geological Expedition, Production Report by V.V. Sivaev and A.F. Goroshko, 1988). (1) Rapakivi of the Ulyalega Massif; (2) massifs of the Hautavaara Complex; (3–5) Shuya Complex; ((3) granite, (4) plagiogranite, tonalite, and granodiorite, (5) diorite); (6) ultramafic rocks of the Hyursul Complex; (7) volcanic and volcano-sedimentary rocks; (8) faults; (9) sampling sites; (10) sampling sites for U–Pb dating.

ero Lake (approximately 5 km) and northward for 3 km. The biotite–hornblende quartz diorites composing this massif are fairly homogeneous in composition and define a compact field in petrochemical diagrams (Fig. 6). The rocks contain 59.28–60.96 wt % SiO_2, belong to the normal-alkalinity series (total of alkalis is 6.02–6.47 wt %) of sodic alkalinity ($Na_2O/K_2O > 1$). The rocks have elevated Mg# = 0.56–0.58. The TiO_2, Al_2O_3, and SiO_2 concentrations of the quartz diorites are intermediate between those in the rocks of the mafic and acid phases of the Hautavaara Massif. The former rocks are richer in CaO and FeO* and poorer in K_2O than the latter ones.

The quartz diorites bear high Cr concentrations (172–188 ppm), are enriched in Ba (634–1459 ppm) and Sr (740–889 ppm), and are contrastingly different from the phase-1 monzodiorites of the Hautavaara Massif in containing high concentrations of Ni (90–99 ppm) and V (111-212 ppm) (Fig. 7).

The REE patterns of the rocks of the Chalka Massif are fractionated: $(La/Yb)_n$ = 11–30. The total REE concentrations are 160–210 ppm. The rocks of the marginal zone are richer in HREE than the quartz diorites in the core of the massif. The PM-normalized multielemental patterns of the quartz diorites resemble those of the rocks of the Hautavaara Massif (Fig. 8).

The granitoids of the ***Shuya Complex***, which were sampled in the eastern and southern parts of the structure, show insignificant variations in their SiO_2 concentrations (67.52–68.96 wt %) at a total concentration of alkalis of 6.81–8.34 wt % and belong to a sodic series ($Na_2O/K_2O > 1$). The shearing of the rocks was associated with their enrichment in biotite and sericite, and hence, in an increase in the concentrations of alkalis and a shift of the rock compositions into the granosyenite field (Fig. 6). According to their petrochemistry (TiO_2, Al_2O_3, FeO*, MgO, and P_2O_5), the rocks of the Shuya Massif correlate with phase 2 of the Hautavaara Massif but differ from the latter in being richer in CaO and poorer in K_2O.

The granodiorites have relatively low Mg# = 0.52–0.43 and bear high concentrations of Cr (53–71 ppm), Ni (24–45 ppm), Ba (460–1270 ppm), and Sr (520–750 ppm) and differ from the phase-2 rocks of the Hautavaara Massif in possessing lower Y, Rb, Zr, and Nb concentrations and higher Sr ones (Fig. 7). The REE patterns of these rocks are strongly fractionated, $(La/Yb)_n$ = 22–30, but the total REE concentrations are relatively low: 103–151 ppm. The normalized multielemental patterns of the granitoids are similar to those of the rocks of the Hautavaara and Chalka Massifs (Fig. 8)

The monzoleucogranites of the Nyalmozero Massif were sampled in its southwestern part and in the area of Nyalmozero Lake. These are highly silicic rocks (SiO_2 = 73.14–73.47 wt %) with elevated concentrations of alkalis (8.36–9.05 wt %) and belong to the sodic series ($Na_2O/K_2O > 1$). The monzoleucogranitoids differ from the granitoids of the aforementioned three massifs in containing lower TiO_2, MgO, and P_2O_5 concentrations (Fig. 6) and having Mg# < 0.50.

The monzoleucogranites are poor in Cr (20–33 ppm), Ni (17–24 ppm), Ti, and V; bear moderately low concentrations of Ba (1330–1653 ppm) and Sr (362–514 ppm); and differ from the granitoids of the Hautavaara, Chalka, and Shuya massifs in containing low V, Zr, Nb, and Y concentrations (Fig. 7).

The rocks have strongly fractionated REE patterns, $(La/Yb)_n$ = 36–85, possess low REE concentrations (45–99 ppm), and are depleted in HREE (Fig. 8).

Table 1. Chemical composition of granitoids in the Hautavaara Structure

Component	1	2	3	4	5	6	7	8
	Hautavaara Massif							
	3/1	3/2	318	330	331	8	370	2
	MGD			MD		QMD		
SiO_2	51.98	53.52	54.45	58.50	57.16	61.74	65.80	65.40
TiO_2	1.03	0.88	0.73	0.67	0.65	0.62	0.50	0.55
Al_2O_3	15.83	15.92	15.29	15.20	14.87	17.66	15.13	14.80
Fe_2O_3	2.91	3.10	3.22	2.27	2.69	2.15	1.35	0.99
FeO	5.46	4.45	4.23	3.59	3.30	2.01	2.15	1.72
MnO	0.144	0.135	0.132	0.111	0.098	0.059	0.058	0.055
MgO	6.74	5.46	5.56	4.70	4.21	2.13	2.38	2.08
CaO	6.82	6.96	6.82	4.91	4.39	1.98	2.04	3.20
Na_2O	2.88	3.49	3.70	3.71	3.50	4.09	3.80	3.91
K_2O	3.33	3.22	3.03	4.02	4.94	6.06	5.61	6.16
P_2O_5	0.61	0.56	0.58	0.42	0.44	0.27	0.10	0.24
LOI	1.72	1.6	1.56	1.63	3.10	1.02	0.94	0.80
Total	99.53	99.51	99.50	99.88	99.64	99.99	99.98	99.96
Mg#	0.60	0.58	0.58	0.60	0.57	0.49	0.56	0.58
alk	6.21	6.71	6.73	7.73	8.44	10.15	9.41	10.07
Na_2O/K_2O	0.86	1.08	1.22	0.92	0.71	0.67	0.68	0.63
Cr	179.9	162.7	166.32	222.5	181.4	53.92	66.3	61.53
Ni	60.64	51.27	56.93	70.1	49.28	22.22	28.5	30.62
V	200.9	178.7	175.88	130.3	127.9	78.64	53.52	104.3
Cu	18.06	35.35	57.07	118.4	61.2	17.67	14.03	14.97
Rb	196.0	120.3	98.3	101.7	226.8	248.26	179.0	290.6
Sr	1032.0	1124.0	1207.62	585.7	692.8	438.02	341.1	328.5
Y	22.61	21.26	19.76	19.25	19.72	23.10	18.16	12.27
Pb	17.63	15.23	24.61	17.64	66.49	14.86	11.22	11.13
Th	4.58	5.49	7.01	12.39	13.65	45.38	49.33	27.47
U	1.47	1.86	2.06	2.01	3.67	4.41	3.59	3.06
Zr	90.31	122.6	69.37	168.4	167.6	457.98	401.7	353.2
Hf	2.19	2.82	2.10	4.13	4.24	11.36	9.34	8.33
Nb	7.95	8.52	5.62	9.75	11.06	24.12	13.35	17.34
Ta	0.38	0.37	0.64	0.58	0.75	2.29	0.93	1.17
Ba	1782.0	2054.0	1751.39	1920.0	1782.0	1224.59	951.1	1003.0
La	41.05	44.93	47.42	45.43	45.19	74.38	47.29	23.03
Ce	97.58	103.5	104.20	92.09	95.75	157.1	104.5	60.27
Pr	12.68	12.56	13.38	10.93	10.86	17.14	10.72	4.83
Nd	55.21	52.72	57.36	41.9	40.26	62.96	41.39	22.59
Sm	12.42	11.43	11.52	7.90	7.57	10.8	8.35	4.80
Eu	3.72	3.58	2.82	2.50	2.34	1.90	1.77	1.09
Gd	10.48	10.19	5.32	7.17	6.86	8.8	5.32	3.60
Tb	1.21	1.12	1.02	0.84	0.82	1.00	0.61	0.46
Dy	4.66	4.29	4.28	3.40	3.47	4.59	2.61	2.81
Ho	0.84	0.80	0.78	0.69	0.70	0.84	0.63	0.53
Er	2.39	2.27	2.04	2.09	2.18	2.38	1.99	1.59
Tm	0.3	0.29	0.25	0.28	0.31	0.34	0.27	0.23
Yb	2.07	2.03	1.81	2.10	2.18	3.60	2.0	1.70
Lu	0.23	0.23	0.23	0.25	0.26	0.36	0.28	0.25

Table 1. (Contd.)

Component	9	10	11	12	13	14	15	16
	Hautavaara Massif							
	5/1	7	327	327/1	350/1	350/2	350/4	350/9
	QMD	GS						
SiO_2	64.93	66.90	69.24	67.02	67.94	68.32	70.60	67.70
TiO_2	0.68	0.48	0.44	0.46	0.39	0.39	0.43	0.43
Al_2O_3	15.80	15.15	13.86	14.47	14.68	14.42	14.40	14.90
Fe_2O_3	1.12	1.18	1.48	1.57	0.73	1.1	1.35	1.05
FeO	2.44	1.94	1.58	2.15	1.68	2.01	0.93	1.86
MnO	0.052	0.054	0.042	0.053	0.051	0.056	0.028	0.052
MgO	2.07	1.92	1.73	2.00	1.65	1.76	1.50	1.86
CaO	2.61	1.83	1.53	1.90	1.60	1.31	0.73	2.0
Na_2O	4.27	3.78	3.26	3.58	4.15	4.93	3.62	3.65
K_2O	4.93	5.55	5.73	5.38	5.42	4.08	4.84	5.55
P_2O_5	0.25	0.22	0.2	0.23	1.32	0.09	0.08	0.06
LOI	0.64	0.76	0.79	0.8	0.07	1.22	1.33	0.78
Total	99.92	99.93	100.0	99.62	99.96	99.82	99.96	99.97
Mg#	0.51	0.54	0.52	0.50	0.56	0.51	0.56	0.54
alk	9.2	9.33	8.99	8.96	9.57	9.01	8.46	9.2
Na_2O/K_2O	0.87	0.68	0.57	0.67	0.77	1.21	0.75	0.66
Cr	74.95	43.36	37.80	44.28	50.96	–	41.11	67.97
Ni	31.34	19.10	18.85	22.06	22.98	–	9.64	32.56
V	138.50	63.80	57.92	66.12	43.72	–	46.88	46.59
Cu	16.84	16.26	12.27	10.30	17.96	–	29.28	18.56
Rb	357.5	217.18	257.22	281.78	226.10	–	203.5	240.5
Sr	598.1	282.82	207.18	420.42	276.0	–	170.7	383.9
Y	9.75	16.46	21.0	20.39	19.94	–	15.32	21.68
Pb	28.42	30.13	21.52	27.29	21.81	–	52.53	23.25
Th	16.04	30.57	28.48	32.48	47.23	–	54.12	54.47
U	5.21	6.96	16.42	11.04	7.52	–	7.24	9.22
Zr	413.0	363.14	328.09	393.98	319.20	–	375.5	316.0
Hf	9.07	8.90	8.09	9.72	8.60	–	9.61	8.21
Nb	12.73	15.87	17.60	18.12	16.14	–	17.62	15.71
Ta	0.43	1.38	2.70	1.94	1.15	–	1.26	1.21
Ba	945.6	1067.19	909.99	915.79	763.0	–	1014.0	805.4
La	33.71	53.26	71.46	55.98	43.87	–	10.17	48.41
Ce	60.23	111.68	139.28	121.76	87.20	–	23.9	106.40
Pr	6.86	12.27	16.13	13.80	9.56	–	2.89	11.47
Nd	30.19	44.88	60.00	51.66	36.77	–	11.85	43.68
Sm	5.66	7.78	10.05	9.35	7.89	–	3.45	9.62
Eu	1.65	1.55	1.61	1.64	1.52	–	0.87	1.72
Gd	3.80	6.47	8.23	7.80	5.68	–	2.84	5.92
Tb	0.45	0.69	0.90	0.86	0.67	–	0.40	0.71
Dy	2.28	3.22	3.89	4.10	2.99	–	2.25	3.11
Ho	0.41	0.56	0.77	0.74	0.73	–	0.57	0.77
Er	1.14	1.62	2.13	2.05	2.13	–	1.76	2.30
Tm	0.16	0.22	0.30	0.28	0.30	–	0.27	0.33
Yb	1.13	2.53	2.79	2.95	2.11	–	1.89	2.26
Lu	0.18	0.25	0.28	0.29	0.28	–	0.24	0.29

Table 1. (Contd.)

Component	17	18	19	20	21	22	23	24
	Hautavaara Massif							
	1	6	319	322	320	320/3	336	352
	GS		MG					
SiO_2	67.74	68.16	70.38	69.46	70.22	70.50	69.32	69.62
TiO_2	0.47	0.43	0.32	0.34	0.34	0.30	0.35	0.35
Al_2O_3	14.93	14.61	14.20	14.14	14.19	14.21	13.98	14.44
Fe_2O_3	0.99	1.42	0.86	1.46	1.15	0.49	1.19	0.92
FeO	1.72	1.72	1.29	1.29	1.22	1.44	1.58	1.79
MnO	0.053	0.045	0.037	0.038	0.035	0.032	0.038	0.043
MgO	1.33	1.55	1.19	1.24	1.03	1.04	1.26	0.71
CaO	1.91	1.76	1.54	1.76	1.32	1.47	1.61	1.60
Na_2O	3.62	3.81	3.78	3.94	3.87	4.21	3.76	3.90
K_2O	5.76	5.43	5.30	5.13	5.50	5.31	5.50	5.20
P_2O_5	0.24	0.2	0.20	0.19	0.22	0.16	0.17	0.07
LOI	0.75	0.72	0.66	0.88	0.59	0.70	0.64	0.83
Total	99.55	100.0	99.89	100.0	99.82	99.98	99.55	99.65
Mg#	0.47	0.48	0.51	0.46	0.45	0.50	0.46	0.33
alk	9.38	9.24	9.08	9.07	9.37	9.52	9.26	9.1
Na_2O/K_2O	0.63	0.7	0.71	0.77	0.70	0.79	0.68	0.75
Cr	51.39	–	20.46	25.92	19.60	–	34.53	47.38
Ni	23.91	–	13.51	14.79	13.95	–	15.11	23.7
V	96.73	–	42.24	40.50	45.73	–	45.73	30.34
Cu	8.37	–	22.78	16.80	5.59	–	10.51	17.47
Rb	371.6	–	239.38	221.38	250.10	–	281.38	212.4
Sr	376.1	–	430.42	424.02	410.82	–	320.18	446.4
Y	16.25	–	14.66	14.10	15.14	–	16.94	13.73
Pb	32.67	–	38.67	17.83	24.74	–	30.40	44.71
Th	30.18	–	37.45	34.31	34.48	–	36.84	43.02
U	7.20	–	11.61	6.30	6.38	–	7.69	8.55
Zr	342.7	–	250.02	224.62	250.41	–	271.37	224.6
Hf	9.11	–	7.03	6.14	6.85	–	7.06	5.86
Nb	16.67	–	13.68	13.27	13.45	–	16.45	11.99
Ta	1.26	–	1.69	1.52	1.61	–	1.77	0.95
Ba	768.5	–	1013.39	1009.79	1080.79	–	863.19	919.3
La	52.46	–	49.66	47.26	49.70	–	44.22	39.07
Ce	86.87	–	103.92	95.56	98.88	–	95.36	73.36
Pr	11.43	–	11.74	10.77	11.59	–	11.32	7.91
Nd	49.47	–	42.76	40.05	42.40	–	41.48	29.32
Sm	8.30	–	7.17	6.80	7.13	–	7.19	6.24
Eu	1.40	–	1.39	1.36	1.38	–	1.24	1.35
Gd	5.23	–	5.94	5.60	5.88	–	6.06	3.81
Tb	0.64	–	0.62	0.60	0.63	–	0.67	0.45
Dy	3.60	–	2.51	2.41	2.55	–	3.16	1.97
Ho	0.65	–	0.53	0.50	0.52	–	0.57	0.48
Er	1.92	–	1.49	1.46	1.48	–	1.66	1.47
Tm	0.28	–	0.22	0.20	0.21	–	0.23	0.21
Yb	1.94	–	2.21	2.00	2.14	–	2.35	1.4
Lu	0.29	–	0.22	0.21	0.21	–	0.24	0.19

Table 1. (Contd.)

Component	25	26	27	28	29	30	31	32	33
	Hautavaara Massif		Chalka Massif						
	363/2	363/3	361	660a	660	661	662	663	665
	MG		QD						
SiO_2	70.32	69.70	59.28	59.9	60.2	60.28	60.94	60.58	60.96
TiO_2	0.39	0.38	0.59	0.57	0.6	0.6	0.57	0.58	0.61
Al_2O_3	13.70	13.90	16.89	16.11	15.95	15.94	15.6	15.69	15.06
Fe_2O_3	0.70	0.84	2.26	2.25	2.15	2.25	2.33	2.27	1.95
FeO	1.43	1.86	3.52	3.52	3.52	3.52	3.45	3.36	4.16
MnO	0.039	0.049	0.107	0.083	0.085	0.105	0.08	0.086	0.093
MgO	1.66	1.62	3.42	4.16	4.16	4.09	4.0	4.21	4.31
CaO	1.60	1.60	5.06	5.12	5.42	5.21	4.77	4.74	4.34
Na_2O	3.88	3.94	3.61	4.26	4.16	4.47	4.16	4.06	3.89
K_2O	5.43	5.10	2.86	1.99	1.86	1.77	2.27	2.39	2.38
P_2O_5	0.11	0.12	0.28	0.31	0.31	0.32	0.29	0.31	0.32
LOI	0.64	0.76	1.41	1.03	0.89	0.82	0.8	0.96	1.27
Total	99.92	99.99	99.51	99.50	99.51	99.57	99.50	99.51	99.52
Mg#	0.59	0.53	0.56	0.57	0.57	0.57	0.56	0.58	0.56
alk	9.31	9.04	6.47	6.25	6.02	6.24	6.43	6.45	6.27
Na_2O/K_2O	0.71	0.77	1.3	2.14	2.24	2.53	1.83	1.70	1.63
Cr	46.28	65.59	116.1	207.1	202.5	171.4	179.8	179.2	144.7
Ni	25.11	36.62	60.47	98.25	97.46	97.38	92.87	94.3	87.82
V	27.82	32.67	111.5	221.6	207.3	211.2	203.9	193.3	195.3
Cu	11.03	13.01	11.57	23.53	25.8	15.29	31.8	23.19	92.82
Rb	151.1	165.0	110.3	64.26	60.7	122.0	76.37	124.6	85.09
Sr	342.4	387.1	679.2	988.2	982.2	861.3	901.2	863.3	822.5
Y	14.55	15.86	17.48	12.99	12.85	19.96	13.11	13.28	12.42
Pb	18.77	10.99	22.02	20.47	19.45	27.07	22.09	20.52	11.58
Th	43.75	43.55	10.15	2.26	2.47	3.35	4.59	5.42	2.68
U	6.16	2.20	1.95	0.42	0.44	3.36	1.31	1.25	1.28
Zr	203.4	229.6	130.9	111.7	153.0	185.1	160.7	172.3	238.3
Hf	5.46	6.21	3.26	2.31	3.06	3.96	3.50	3.63	4.56
Nb	10.93	11.89	5.55	4.33	4.39	9.78	5.06	5.35	5.28
Ta	0.97	1.03	0.52	0.51	0.54	1.16	0.61	0.65	0.64
Ba	884.1	836.7	977.2	582.4	534.3	338.7	558.5	579.0	743.0
La	30.87	41.53	46.32	30.19	44.67	29.83	44.74	43.70	29.32
Ce	66.37	73.63	85.77	83.67	99.64	79.78	100.90	101.30	77.29
Pr	8.00	9.66	10.26	9.70	11.98	9.54	11.81	11.86	8.98
Nd	31.21	37.55	38.67	40.14	45.59	38.78	44.73	45.69	37.23
Sm	6.59	7.55	6.14	6.79	6.96	6.84	7.06	7.13	6.35
Eu	1.44	1.54	1.62	1.76	1.79	1.68	1.78	1.88	1.72
Gd	4.09	4.50	4.61	4.92	4.94	5.28	5.02	5.15	4.63
Tb	0.49	0.54	0.69	0.57	0.59	0.68	0.62	0.60	0.55
Dy	2.16	2.40	3.20	2.71	2.66	3.31	2.69	2.80	2.63
Ho	0.52	0.59	0.60	0.50	0.48	0.61	0.47	0.49	0.49
Er	1.58	1.71	1.72	1.28	1.27	1.76	1.27	1.29	1.24
Tm	0.21	0.24	0.25	0.17	0.16	0.27	0.16	0.17	0.16
Yb	1.53	1.65	1.62	1.06	1.07	1.94	1.10	1.13	1.09
Lu	0.20	0.21	0.26	0.15	0.15	0.29	0.16	0.16	0.16

Table 1. (Contd.)

Component	34	35	36	37	38	39	40	41	42
	Shuya Massif					Nyalmozero Massif			
	524	526	650	651	2*	353	676	677	678
	GD					MLG			
SiO_2	68.16	68.20	67.52	67.62	68.96	73.14	73.4	73.44	73.47
TiO_2	0.30	0.34	0.37	0.41	0.36	0.13	0.10	0.09	0.10
Al_2O_3	15.31	15.08	15.20	15.09	14.99	13.63	14.60	14.60	14.60
Fe_2O_3	1.33	1.39	1.61	2.02	3.21	0.13	0.36	0.39	0.40
FeO	1.44	1.51	1.51	1.51	–	1.0	1.15	0.57	0.93
MnO	0.061	0.054	0.050	0.047	0.06	0.026	0.016	0.012	0.013
MgO	1.41	1.42	1.74	2.05	1.22	0.78	0.35	0.41	0.30
CaO	2.01	2.58	2.39	2.82	2.36	1.31	1.37	1.30	1.16
Na_2O	4.43	4.27	4.24	5.64	4.36	4.14	4.47	4.52	4.37
K_2O	3.88	3.60	4.10	1.17	2.99	4.91	3.89	4.16	4.16
P_2O_5	0.17	0.20	0.24	0.25	0.13	0.06	0.05	0.05	0.03
LOI	1.28	1.01	0.88	1.18	0.82	0.32	0.08	0.29	0.30
Total	100.0	99.98	100.0	99.98	99.46	99.97	99.99	99.95	100.0
Mg#	0.49	0.48	0.51	0.52	0.43	0.55	0.29	0.44	0.29
alk	8.31	7.87	8.34	6.81	7.35	9.05	8.36	8.68	8.53
Na_2O/K_2O	1.14	1.19	1.03	4.82	1.46	0.84	1.15	1.09	1.05
Cr	52.68	61.12	57.90	71.0	–	33.63	19.58	22.68	26.32
Ni	24.24	35.45	37.38	45.31	–	19.25	16.58	23.09	24.15
V	40.74	50.08	36.97	40.89	–	<DL	<DL	<DL	<DL
Cu	10.67	3.61	17.80	23.50	–	5.61	11.77	7.54	11.30
Rb	110.60	94.60	89.41	31.51	–	85.68	103.50	101.60	103.20
Sr	520.30	749.80	607.30	620.80	–	369.20	362.00	396.70	514.10
Y	8.84	10.17	7.59	9.62	–	2.87	2.88	1.79	1.14
Pb	12.62	15.55	14.29	11.12	–	22.92	26.02	27.66	21.14
Th	9.97	10.29	9.48	16.89	–	11.46	9.94	11.74	8.25
U	1.47	1.84	5.37	2.21	–	0.75	0.97	0.72	0.58
Zr	111.30	150.60	115.70	129.30	–	85.39	75.75	70.17	70.78
Hf	3.19	4.10	2.89	2.97	–	2.54	2.26	1.94	1.99
Nb	6.46	6.54	5.10	5.24	–	2.17	1.58	1.39	1.36
Ta	0.65	0.60	0.45	0.44	–	0.16	0.06	0.07	0.05
Ba	1257.0	1274.0	1252.0	457.3	–	1518.0	1330.0	1385.0	1653.0
La	26.91	33.67	21.40	27.02	–	15.20	27.51	9.63	16.06
Ce	45.93	61.27	46.34	76.01	–	29.17	45.60	21.77	31.04
Pr	7.18	9.13	5.06	6.28	–	2.97	4.27	1.84	2.68
Nd	25.16	31.90	19.2	22.79	–	10.69	15.63	7.94	9.87
Sm	4.55	5.50	3.64	4.13	–	2.08	2.50	1.70	1.69
Eu	1.21	1.42	1.12	1.16	–	0.78	0.68	0.65	0.68
Gd	2.89	3.61	2.80	3.24	–	1.33	1.43	0.91	0.72
Tb	0.42	0.41	0.38	0.42	–	0.14	0.19	0.11	0.08
Dy	1.81	1.96	1.66	2.00	–	0.52	0.70	0.39	0.28
Ho	0.34	0.36	0.26	0.31	–	0.11	0.10	0.06	0.04
Er	0.87	0.95	0.78	0.92	–	0.30	0.25	0.18	0.13
Tm	0.11	0.13	0.12	0.14	–	0.04	0.03	0.02	0.02
Yb	0.76	0.84	0.71	0.82	–	0.23	0.23	0.19	0.17
Lu	0.13	0.13	0.12	0.11	–	0.04	0.04	0.03	0.02

(6–10) According to (Dmitrieva et al., 2016). Rock symbols: GD—granodiorite, GS—granosyenite, D—diorite, QD—quartz diorite, QMD—quartz monzodiorite, LG—leucogranite, MG—monzogranite, MGD—monzogabbrodiorite, MD—monzodiorite, MLG—monzoleucogranite. Oxides are in wt %, elements are in ppm, <DL means concentrations below the detection limits, dashes mean not analyzed, Mg# = $Mg/(Fe^{2+} + Fe^{3+} + Mg)$. *Data provided by the Karelian Geological Expedition.

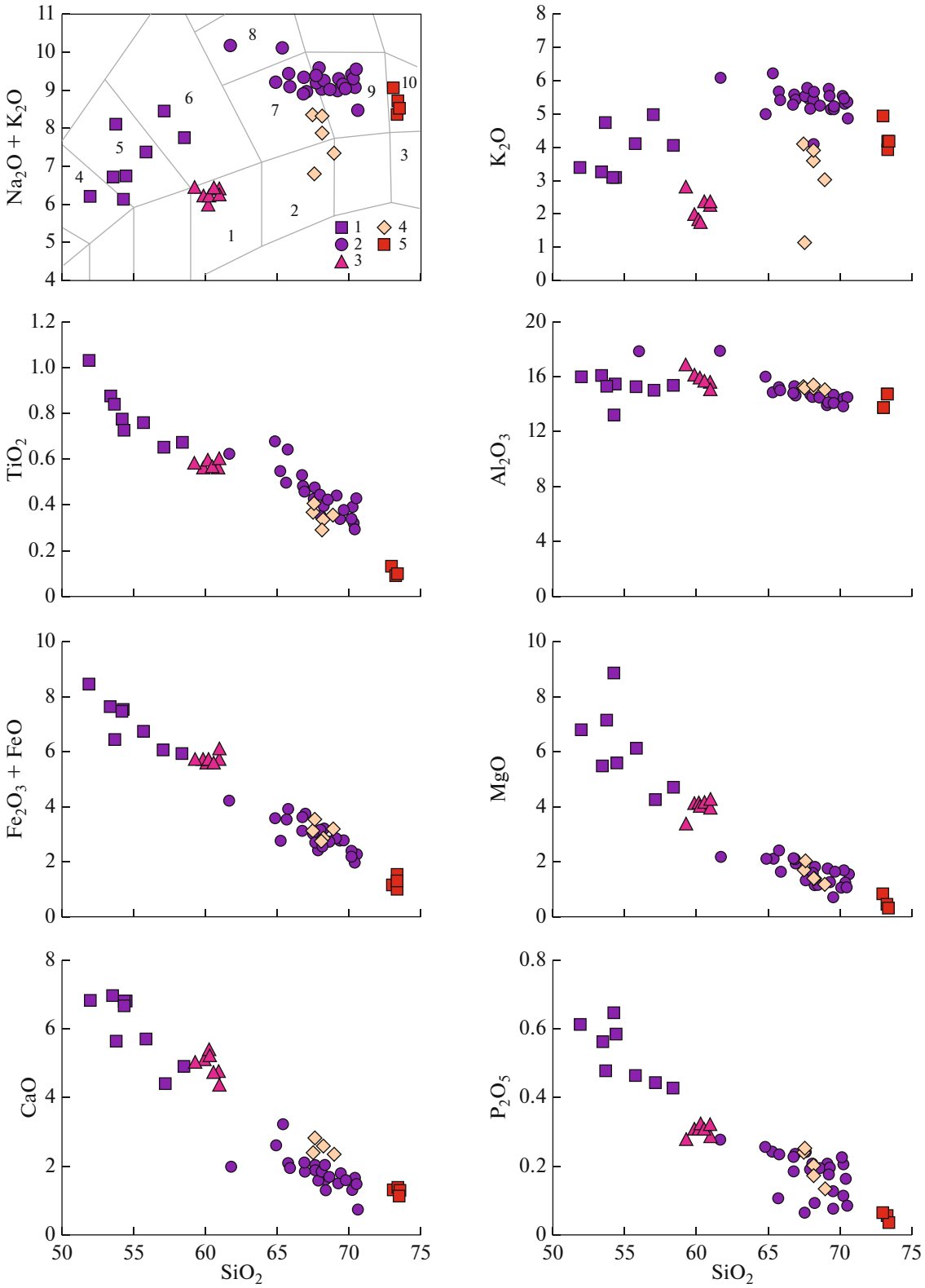

Fig. 6. Harker diagrams for granitoids of the Hautavaara Structure. Massifs: (1, 2) Hautavaara ((1) phase 1, (2) phase 2); (3) Chalka; (4) Shuya; (5) Nyalmozero. Composition fields are given according to (Sharpenok et al., 2013): (1) quartz diorite, (2) granodiorite, (3) leucogranite, (4) monzogabbrodiorite, (5) monzodiorite, (6) monzonite, (7) granosyenite, (8) syenite, (9) mildly alkaline granite, (10) mildly alkaline leucogranite.

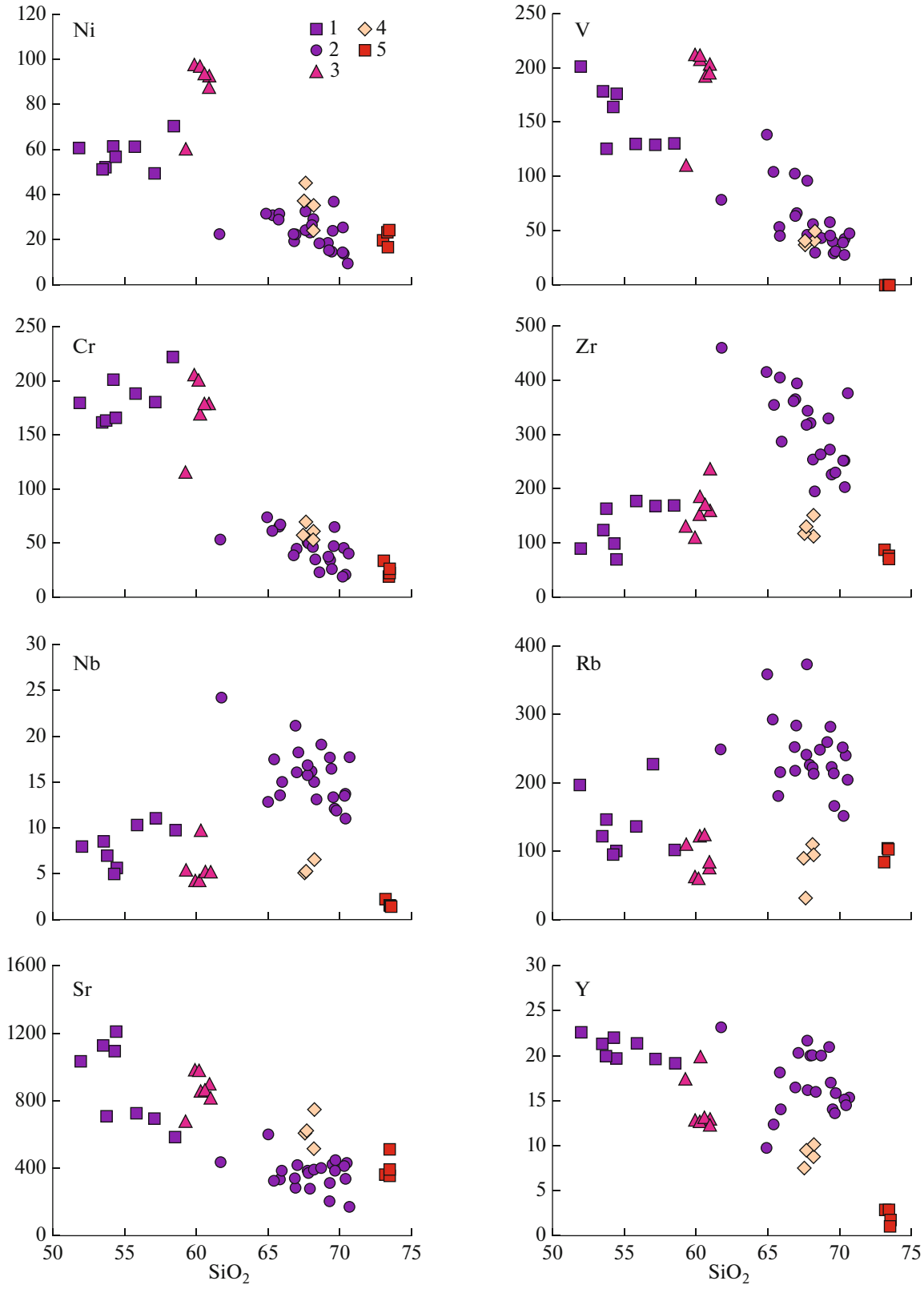

Fig. 7. Diagrams SiO_2 vs. Ni, V, Cr, Zr, Nb, Rb, Sr, and Y for granitoids of the Hautavaara Structure. Massifs: (1, 2) Hautavaara ((1) phase 1, (2) phase 2); (3) Chalka; (4) Shuya; (5) Nyalmozero.

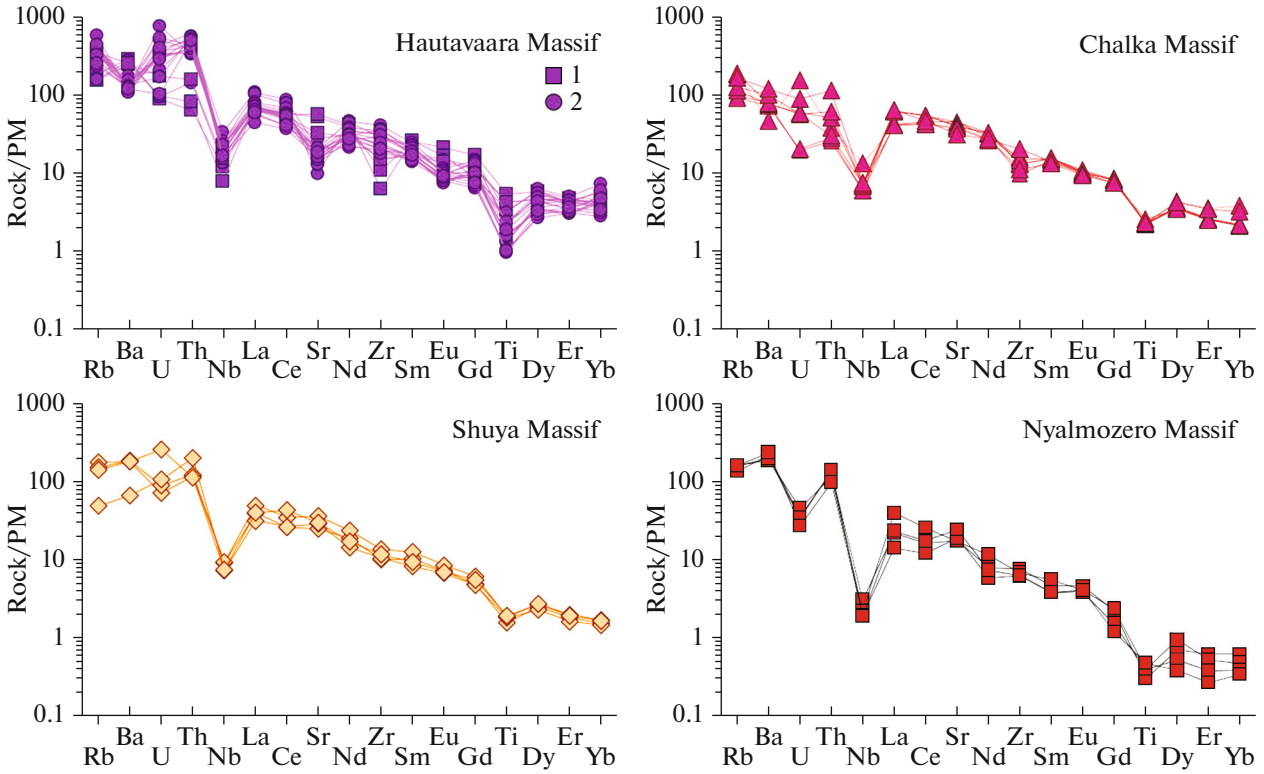

Fig. 8. Primitive mantle-normalized (Sun and McDonough, 1989) multielemental patterns for granitoids of the Hautavaara Structure. (1) Phase 1, (2) phase 2.

U–Pb ISOTOPE ZIRCON GEOCHRONOLOGY

The U–Pb age values of rocks of the various magmatic phases of the ***Hautavaara Massif*** were published in (Bibikova et al., 2005; Stepanova et al., 2014) (see above).

Pale brown prismatic zircon crystals and their fragments with variable crystal faceting and thin oscillatory zoning (Fig. 9a) were separated from the quartz diorite of the ***Chalka Massif*** (sample 660). The zircon grains are 200–300 μm long, and their $^{232}Th/^{238}U$ ratio varies from 0.56 to 0.79 and corresponds to that of magmatic zircon.

The $^{206}Pb/^{238}U$–$^{207}Pb/^{235}U$ diagrams (Fig. 10) show that the zircons yield a concordant age of 2739.1 ± 6.9 Ma (MSWD = 0.57, n = 10), which corresponds to the crystallization age of the quartz diorites of the Chalka Massif. This age value is consistent with that determined previously by the classic method: 2745 ± 5 Ma (Ovchinnikova et al., 1994).

The dominant zircons in the granitoids of the ***Shuya Massif*** are pale brown short- and long-prismatic euhedral grains (sample 650a) with variably preserved oscillatory zoning (Fig. 9b). The crystals are 200–400 μm long. The CL images of some of the zircons show paler euhedral cores with clearly seen magmatic sectorial zoning (grains 1–3 and 10). Some of the crystals display relict oscillatory zoning and a homogeneous inner structure.

Fifteen spot analyses for isotope concentrations of ten zircon crystals (in their cores and margins) were used to calculate the isotope ratios (Table 2). The $^{232}Th/^{238}U$ = 0.50–0.83. The oldest age value of 2863 ± 31 was determined in grain 7 and correlates with the emplacement age of the subvolcanic rhyolite porphyry dikes: 2862 ± 45 Ma (Ovchinnikova et al., 1994). This zircon grain seems to be xenogenic and was thus rejected from further considerations. The age values are slightly scattered in the Ahrens–Wetherill diagram (Fig. 10). Six of the data points make up a compact cluster ($-1 < D < 1$) corresponding to an age of 2745 ± 10 Ma, concordance MSWD = 0.047, concordance probability = 0.83. Three spot analyses (the core and margin of grain 4 and the core of grain 6) are discordant and plot below the concordia ($19 < D < 42$). The deviations from the concordia are explained by the losses of radiogenic Pb. Five spots (the core of grain 2 and the outer zones of grains 1, 3, 5, and 10) are subconcordant ($4 < D < 6$). All of the calculated age values plot on a linear trend (discordia), which implies that the zircons are syngenetic. The upper intercept of the concordia and discordia corresponds to an age of 2745.7 ± 7.6 Ma (MSWD = 0.83), and the lower intercept involves a large error.

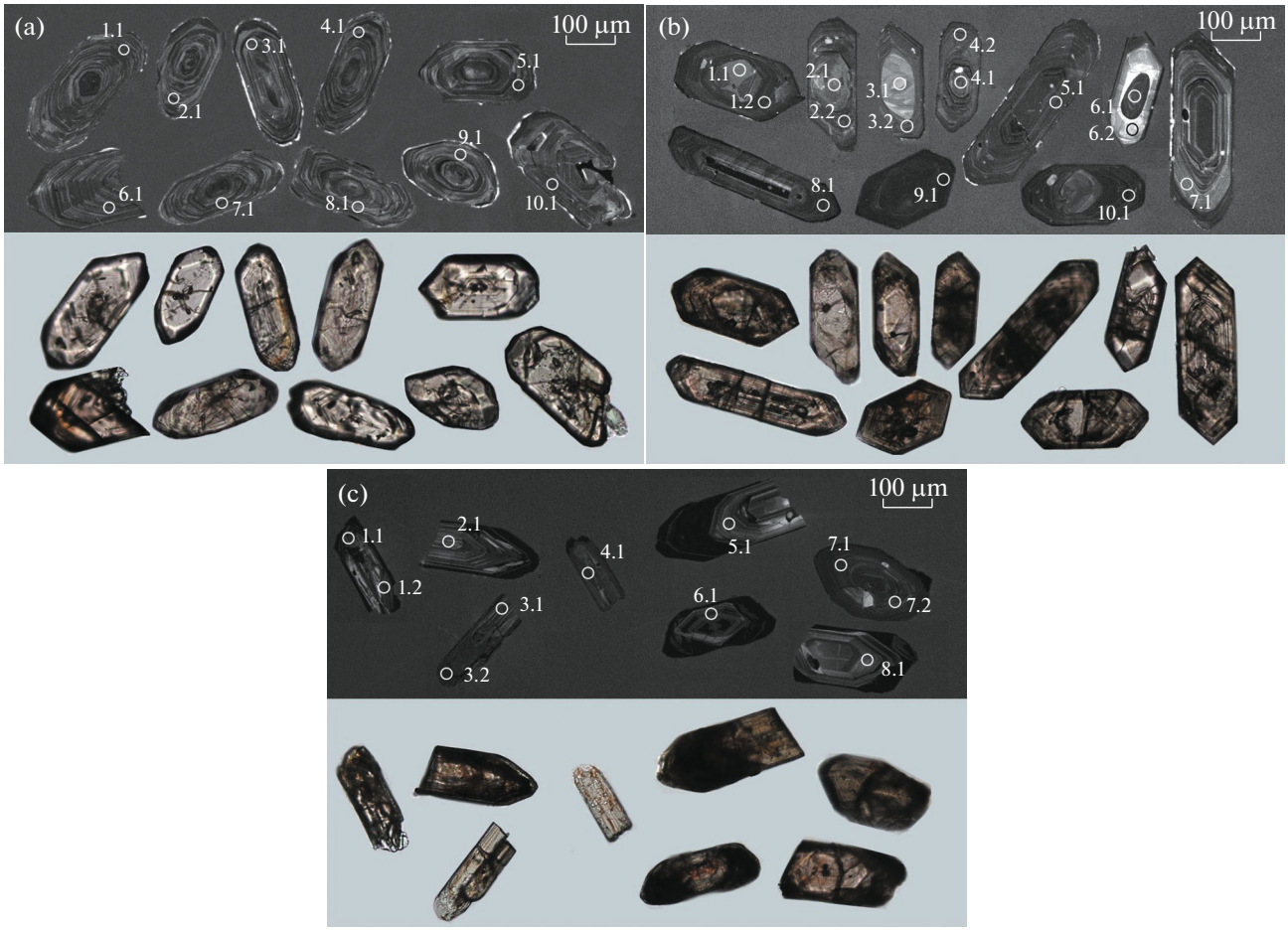

Fig. 9. Optical micrographs and CL images of the zircons. Massifs: (a) Chalka , sample 660; (b) Shuya , sample 650-a; (c) Nyalmozero , samples 676–678.

Data on zircons from granitoids of the Shuya Massif indicate that most of the zircon cores are not xenogenic (do not yield old age values and show well-preserved euhedral morphologies). The possible mechanism of their origin was crystallization from magma, which triggered the partial melting of the preexisting crystals and their overgrowing with newly formed outer zones under lower pressures. The analyzed cores and margins yield consistent age values. The core of grain *6* differs from the other crystals, is ellipsoidal, and may be of inherited nature. Nevertheless, the age value calculated for spot 6.1 plots on a discordia, which suggests that the U–Pb systems has been completely reequilibrated.

Zircons from the monzoleucogranites of the ***Nyalmozero Massif*** are transparent and semitransparent prismatic crystals of various size and their fragments (samples 676–678, Fig. 9c). The grains are 155–290 μm long. The CL images of the zircons show their coarse zoning. Their $^{232}Th/^{238}U = 0.21–0.75$. Isotope concentrations were measured at eleven spots at these grains. Spot 3.2 (margin of a grain) was rejected because of its very high U concentration ($^{232}Th/^{238}U = 0.01$) and elevated content of radiogenic Pb; the calculated concordant age is younger and plots away from the intercept of the discordia and concordia.

In the concordia diagram, the age values are slightly scattered (Fig. 10). Four of the spots have highly discordant isotope ratios ($10 < D < 22$), three are subconcordant ($2 < D < 3$), and three others lie on the concordia. The regression line for all of the calculated values has an upper intercept with the concordia corresponding to an age of 2740.9 ± 9.4 Ma (MSWD = 0.84). The data points plotting on the concordia (three ellipses) were used to calculate an age value of 2737 ± 13 Ma (MSWD = 0.048, concordance = 0.83). The weighted mean age value calculated based on the $^{207}Pb/^{206}Pb$ ratio is 2739.3 ± 8.3 Ma (Fig. 11).

Sm–Nd ISOTOPE DATA

The rocks of the ***Hautavaara Massif*** have $\varepsilon_{Nd}(2.74) = +0.1$ to $+1.1$ (Lobach-Zhuchenko et al., 2000; Kovalenko et al., 2005; and Yu.S. Egorova's data, personal communication). The ε_{Nd} value close to zero implies that the melt source might have been produced by

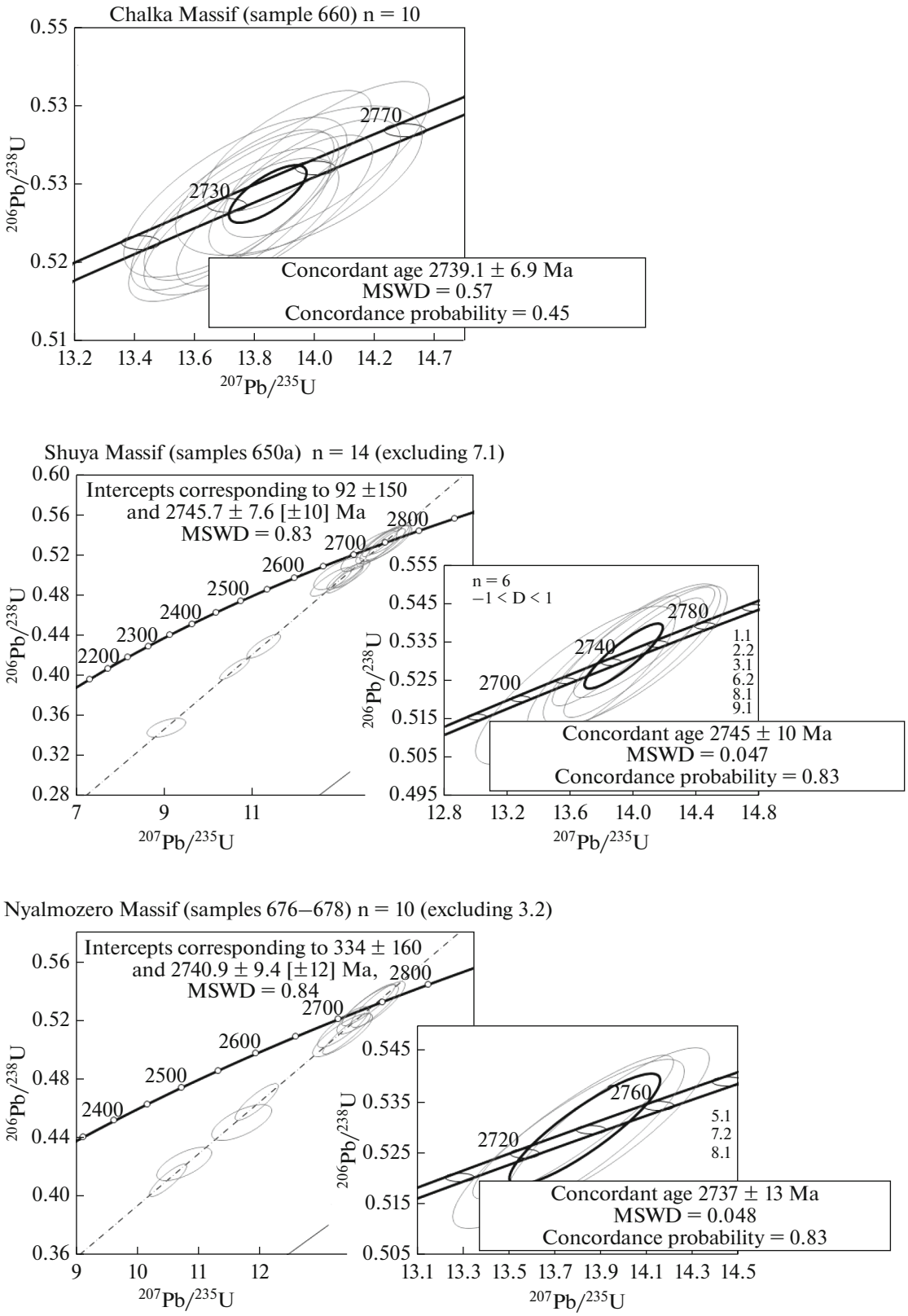

Fig. 10. Ahrens–Wetherill concordia diagrams showing the ellipses of errors, for the zircon ages of granitoid massifs in the Hautavaara Structure. The ellipses and concordant age values are presented with 2σ errors.

Table 2. U–Pb isotope data on zircons from granitoids of the Hautavaara Structure

Grain, spot	$^{206}Pb_c$, %	Concentration, ppm		$^{232}Th/^{238}U$	$^{206}Pb^*$, ppm	Age ± 1σ, Ma		D, %	$^{238}U/^{206}Pb^*$ ± %	$^{207}Pb^*/^{206}Pb^*$ ± %	$^{207}Pb^*/^{235}U$ ± %	$^{206}Pb^*/^{238}U$ ± %	CC
		U	Th			$^{206}Pb/^{238}U$	$^{207}Pb/^{206}Pb$						
Chalka Massif (sample 660, quartz diorite)													
1.1	0.03	155	95	0.63	71.2	2755 ± 17	2751 ± 11	0	1.876 ± 0.8	0.191 ± 0.6	14.04 ± 1.0	0.5331 ± 0.8	0.8
2.1	0.02	168	104	0.64	76.1	2727 ± 16	2752 ± 10	1	1.899 ± 0.7	0.1911 ± 0.6	13.87 ± 1.0	0.5266 ± 0.7	0.8
3.1	0.12	171	95	0.58	77.6	2730 ± 16	2736 ± 10	0	1.897 ± 0.7	0.1893 ± 0.6	13.76 ± 1.0	0.5272 ± 0.7	0.8
4.1	0.04	152	83	0.56	68.4	2719 ± 15	2744 ± 11	1	1.906 ± 0.7	0.1902 ± 0.7	13.76 ± 1.0	0.5246 ± 0.7	0.7
5.1	0.02	205	131	0.66	94.3	2759 ± 13	2732 ± 9	– 1	1.872 ± 0.6	0.1889 ± 0.6	13.91 ± 0.8	0.5341 ± 0.6	0.7
6.1	0.05	150	91	0.63	68	2728 ± 18	2734 ± 11	0	1.899 ± 0.8	0.189 ± 0.7	13.73 ± 1.0	0.5267 ± 0.8	0.8
7.1	0.05	159	118	0.76	71.7	2719 ± 17	2738 ± 11	1	1.906 ± 0.8	0.1896 ± 0.7	13.72 ± 1.0	0.5248 ± 0.8	0.8
8.1	0.09	113	76	0.69	51.3	2734 ± 17	2731 ± 13	0	1.893 ± 0.8	0.1887 ± 0.6	13.74 ± 1.1	0.5283 ± 0.8	0.7
9.1	0.10	129	80	0.64	58.8	2743 ± 16	2749 ± 16	0	1.885 ± 0.7	0.1908 ± 1.0	13.95 ± 1.2	0.5304 ± 0.7	0.6
10.1	0.03	158	120	0.79	71.8	2740 ± 15	2753 ± 11	1	1.888 ± 0.7	0.1913 ± 0.7	13.97 ± 0.9	0.5295 ± 0.7	0.7
Shuya Massif (sample 650a, granodiorite)													
1.1	0.08	76	60	0.83	34.5	2748 ± 30	2752 ± 16	0	1.882 ± 1.4	0.1912 ± 1.0	14.01 ± 1.7	0.5314 ± 1.4	0.819
1.2	0.57	173	95	0.57	73.5	2585 ± 26	2723 ± 13	5	2.027 ± 1.2	0.1878 ± 0.8	12.77 ± 1.5	0.4932 ± 1.2	0.189
10.1	0.24	226	149	0.68	97.3	2616 ± 24	2756 ± 11	5	1.998 ± 1.1	0.1916 ± 0.7	13.22 ± 1.3	0.5005 ± 1.1	0.192
2.1	2.34	146	94	0.67	64.3	2620 ± 28	2719 ± 20	4	1.995 ± 1.3	0.1874 ± 1.2	12.95 ± 1.8	0.5013 ± 1.3	0.187
2.2	0.05	232	137	0.61	106	2762 ± 25	2748 ± 10	– 1	1.869 ± 1.1	0.1907 ± 0.6	14.07 ± 1.3	0.5349 ± 1.1	0.191
3.1	0.03	71	48	0.69	32.5	2744 ± 34	2746 ± 16	0	1.884 ± 1.5	0.1905 ± 1.0	13.94 ± 1.8	0.5307 ± 1.5	0.190
3.2	0.27	237	139	0.61	102	2608 ± 24	2744 ± 10	5	2.005 ± 1.1	0.1903 ± 0.6	13.08 ± 1.3	0.4986 ± 1.1	0.190
4.1	5.61	354	232	0.68	112	1925 ± 18	2729 ± 26	42	2.874 ± 1.1	0.1885 ± 1.6	9.04 ± 2.0	0.3479 ± 1.1	0.188
4.2	0.60	280	154	0.57	98.4	2199 ± 21	2732 ± 11	24	2.46 ± 1.1	0.1888 ± 0.7	10.58 ± 1.3	0.4065 ± 1.1	0.189
5.1	0.04	257	125	0.50	109	2595 ± 25	2754 ± 9	6	2.018 ± 1.1	0.1913 ± 0.6	13.08 ± 1.3	0.4956 ± 1.1	0.191
6.1	1.12	264	157	0.62	98.3	2302 ± 21	2742 ± 13	19	2.331 ± 1.1	0.1899 ± 0.8	11.24 ± 1.4	0.4291 ± 1.1	0.190
6.2	0.07	75	40	0.55	33.9	2715 ± 35	2732 ± 17	1	1.909 ± 1.6	0.1888 ± 1.0	13.63 ± 1.9	0.5237 ± 1.6	0.189
8.1	0.07	232	150	0.67	106	2745 ± 26	2753 ± 10	0	1.883 ± 1.2	0.1913 ± 0.6	14 ± 1.3	0.5309 ± 1.2	0.191
9.1	0.04	284	214	0.78	130	2753 ± 25	2734 ± 9	– 1	1.877 ± 1.1	0.1891 ± 0.5	13.89 ± 1.2	0.5327 ± 1.1	0.189
7.1	0.04	98	56	0.59	47.1	2863 ± 31	2867 ± 14	0	1.788 ± 1.3	0.2051 ± 0.9	15.81 ± 1.6	0.5592 ± 1.3	0.205
Nyalmozero Massif (samples 676–678, monzoleucogranite)													
3.1	0.70	394	287	0.75	140	2217 ± 20	2702 ± 10	22	2.436 ± 1.1	0.1854 ± 0.6	10.5 ± 1.2	0.4105 ± 1.1	0.9
1.1	4.53	253	57	0.23	96.1	2268 ± 22	2701 ± 21	19	2.371 ± 1.1	0.1853 ± 1.3	10.77 ± 1.7	0.4217 ± 1.1	0.7
1.2	2.17	231	48	0.21	91.1	2394 ± 23	2732 ± 21	14	2.223 ± 1.1	0.1889 ± 1.3	11.71 ± 1.7	0.4498 ± 1.1	0.7
6.1	0.66	290	122	0.43	116	2457 ± 22	2714± 10	10	2.155 ± 1.1	0.1868 ± 0.6	11.95 ± 1.2	0.4640 ± 1.1	0.9
2.1	0.23	120	55	0.47	52.7	2655 ± 27	2743 ± 13	3	1.962 ± 1.2	0.1901 ± 0.8	13.36 ± 1.5	0.5096 ± 1.2	0.8
7.1	0.17	353	222	0.65	155	2658 ± 24	2748 ± 8	3	1.959 ± 1.1	0.1907 ± 0.5	13.42 ± 1.2	0.5104 ± 1.1	0.9
4.1	0.83	245	156	0.66	109	2678 ± 24	2728 ± 11	2	1.942 ± 1.1	0.1883 ± 0.7	13.37 ± 1.3	0.5150 ± 1.1	0.9
3.2	0.03	1549	11	0.01	687	2683 ± 21	2702 ± 4	1	1.938 ± 1.0	0.18544 ± 0.2	13.2 ± 1.0	0.5161 ± 1.0	1.0
8.1	0.06	128	38	0.31	57.9	2728 ± 29	2737 ± 13	0	1.898 ± 1.3	0.1895 ± 0.8	13.76 ± 1.5	0.5268 ± 1.3	0.9
7.2	0.06	243	127	0.54	111	2742 ± 25	2729 ± 9	0	1.886 ± 1.1	0.1885 ± 0.5	13.78 ± 1.3	0.5302 ± 1.1	0.9
5.1	0.16	160	53	0.34	72.8	2743 ± 26	2746 ± 11	0	1.886 ± 1.2	0.1905 ± 0.7	13.93 ± 1.3	0.5303 ± 1.2	0.9

Errors at ±1σ, Pb_c and Pb^* are common and radiogenic Pb, respectively, correlation by ^{204}Pb, D is discordance: $D = 100 \times [age(^{207}Pb/^{206}Pb)/age(^{206}Pb/^{238}U)]$, CC is the correlation coefficient between the errors of the $^{206}Pb/^{235}U$ and $^{207}Pb/^{235}Pb$ isotope ratios.

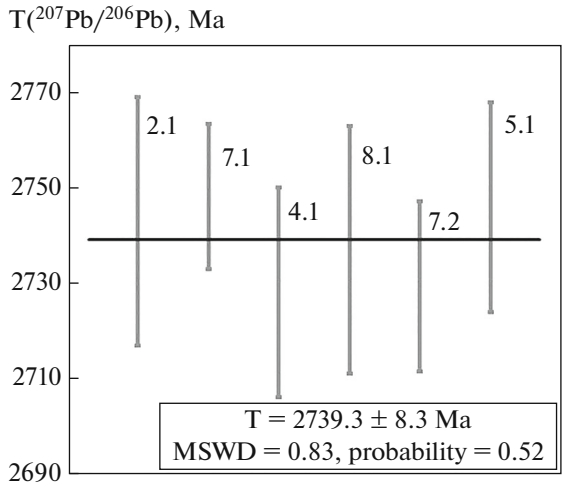

Fig. 11. Weighted mean $^{207}Pb/^{206}Pb$ zircon age of the Nyalmozero Massif.

mixing depleted mantle and crustal materials. Some samples of the phase-2 monzodiorites have a more radiogenic Nd isotope composition: ε_{Nd} up to +1.1. The model age of the rocks $T_{Nd}(DM) \sim 3$ Ga.

The quartz diorites of the ***Chalka Massif*** have $\varepsilon_{Nd}(2.74) = +0.4$ (Table 3). A value of $\varepsilon_{Nd}(2.74) = -1.3$ has been obtained for this massif in (Kovalenko et al., 2005).

The granodiorites of the ***Shuya Massif*** have negative $\varepsilon_{Nd}(2.74) = -2.8$, which corresponds to a crustal source. The model age $T_{Nd}(DM)$ calculated according to the model (Goldstein and Jacobsen, 1988) is 3.2 Ga.

The monzoleucogranites of the ***Nyalmozero Massif*** also have negative $\varepsilon_{Nd}(2.74) = -1.0$ nad $T_{Nd}(DM) = 3.1$.

DISCUSSION

The data presented above enable discussion of the age and genetic relationships of Neoarchean granitoids in the Hautavaara Structure and the source and tectonic environments in which their parental melts were derived.

U–Pb Zircon Geochronology and Age Correlations between the Granitoids of Massifs in the Hautavaara Structure

The U–Pb zircon ages of the compositionally different granitoids append the results of earlier studies of the Hautavaara Structure.

The Hautavaara sanukitoid massif in the central part of the Hautavaara Structure is a most exhaustively studied reference intrusion, whose monzodiorites and granosyenites of different intrusive phases (which were sampled in different parts of the massif) were dated by ID-TIMS (Stepanova et al., 2014) and SIMS (Bibikova et al., 2005) methods. The dates lie within the range of 2735–2743 Ma and are the reliably justified age of emplacement of this polyphase sanukitoid massif.

The Chalka Massif of diorites of the sanukitoid series in the northwestern surroundings of the Hautavaara Structure has an U–Pb zircon age (SHRIMP-II) of 2739 ± 7 Ma and an U–Pb zircon age of 2745 ± 5 Ma (classic technique) (Ovchinnikova et al., 1994). This age coincides with the age of diorites of the Hautavaara sanukitoid massif.

The Shuya tonalite–granodiorite massif in the southeastern surroundings of the Hautavaara Structure was previously viewed as a probable member of the much older tonalite–trondhjemite–granodiorite series of granitoids dated at approximately 2.85 Ga (Kuleshevich et al., 2009). The U–Pb zircon age of a granodiorite sample from this massifs reliably determines its age as 2745 Ma, which makes this massif coeval with the Hautavaara and Chalka sanukitoid massifs. One older zircon grain identified in the zircon population has a $^{207}Pb/^{206}Pb$ age of 2863 Ma and was likely entrapped by the granitoid magma from the volcanic rocks or TTG granitoids of the Hautavaara Structure.

The Nyalmozero Massif in the northeastern surroundings of the Hautavaara Structure is thought to represent the younger leucogranites, which were dated elsewhere in the Karelian Craton at 2.70–2.68 Ga (Höltta et al., 2012; Chekulaev et al., 2020). Our data indicate that most zircon grains from the leucogranite of this massif have an age of 2741 Ma, which likely cor-

Table 3. Sm–Nd isotope data on granitoids of the Hautavaara Structure

Sample	T_{Zr}, Ma	Sm, ppm	Nd, ppm	$^{147}Sm/^{144}Nd$	$^{143}Nd/^{144}Nd$	±	$\varepsilon_{Nd}(T)$	$T_{Nd}(DM)$
Chalka Massif (quartz diorite, diorite)								
660	2739	6.93	43.79	0.0957	0.510834	2	0.4	2.97
Shuya Massif (granodiorite)								
650a	2745	4.39	24.28	0.1094	0.510913	3	−2.8	3.25
Nyalmozero Massif (monzoleucogranite)								
676	2737	1.35	8.61	0.0945	0.510744	4	−1.0	3.06

T_{Zr} is the U–Pb zircon age, $T_{Nd}(DM)$ is the model age relative to the depleted mantle (Goldstein and Jacobsen, 1988).

responds to the age of the rock and overlaps with the ages of the other granitoid massifs in the Hautavaara Structure. One analytical spot in the marginal portion of a younger grain with a $^{207}Pb/^{206}Pb$ age of 2702 Ma has very high concentrations of U and radiogenic Pb and seems to reflect the disturbance of the U–Pb system of the zircon.

Our geochronologic study thus shows that the Hautavaara Structure was simultaneously intruded by sanukitoid massifs and small tonalite–granodiorite and leucogranite intrusions at 2.74 Ga. The age range of 2735–2745 Ma of this granitic magmatism in the southern part of the Vedlozero–Segozero Greenstone Belt is consistent with that rocks produced by younger granitoid magmatism are found in the western part of the Karelian Craton, where sanukitoids and compositionally diverse granites were dated at 2.72–2.68 Ma (Höltta et al., 2012; Chekulaev et al., 2020) and are younger than the granite magmatism in the eastern part of the Karelian Craton in the surroundings of the Vodlozero Domain.

Genetic Relationships between Granitoids in the Hautavaara Structure

The data we obtained on the undiscernibly similar ages of all granitoid massifs studied in the Hautavaara Structure and the newly acquired petrographic, geochemical, and isotope data provide grounds for discussing possible genetic relationships between the parental magmas of these rocks.

The origin of the granitoids of different composition and their genetic relationships are most actively discussed with reference to polyphase sanukitoid massifs, such as the Hautavaara Massif, which contains diorites and monzogranites.

Currently all researchers are prone to believe that the mafic rocks of sanukitoid series are generated by the melting of a mantle source that was metasomatized by acid melts (Rapp et al., 1999, 2010; Martin et al., 2009; Samsonov et al., 2004; Larionova et al., 2007) or H_2O and/or CO_2 fluid (Lobach-Zhuchenko et al., 2008; Mikkola et al., 2011). For the Hautavaara and Chalka massifs, this mechanism realistically explains geochemical features of the diorites, which are both rich in Cr and Ni (which implies a mantle source of the magmas) and bear Ba, Sr, HFSE, and LREE concentrations that are unusually high for mantle melts.

The derivation of acid rocks of the sanukitoid series, including those at the Karelian Craton, is often thought to be related to the crystallization differentiation of more mafic magmas (Stern and Hanson, 1991; Samsonov et al., 2004; Lobach-Zhuchenko et al., 2005, 2008) or is sometimes explained by the mixing of mantle mafic magmas and crustal granitic melts (Laurent et al., 2014 and references therein). The quartz diorites and monzogranites of the Hautavaara Massif have geochemical features of sanukitoid series, such as elevated concentrations of Ba, Sr, and HFSE, and can thus be viewed as differentiation products of more mafic sanukitoid magmas. This is consistent with the radiogenic Nd isotope composition of the monzogranites and syenites [$(\varepsilon_{Nd}(T) = 0.08–0.61$; Kovalenko et al., 2005], which is comparable to the Nd isotope composition of mafic rocks [$(\varepsilon_{Nd}(T) = 0.08–0.74$; Kovalenko et al., 2005 and this publication] and does not imply that any appreciable amounts of older crustal material were added.

The monzogranites of the Hautavaara Massif possess geochemical features that make them different from most sanukitoids in the Karelian and other cratons. For example, the transition between the mafic and acid phases in many two-phase sanukitoid massifs is associated with a decrease in the HREE concentrations at unchanging concentrations of Al_2O_3, which is explained by the fractionation of hornblende at a subordinate role of plagioclase in the cumulus association and suggests that the sanukitoid melts possessed elevated H_2O concentrations (Stern et al., 1989; Samsonov et al., 2004). Conversely, the monzogranites of the Hautavaara Massif have HREE concentrations similar to those in the diorites but are poorer in Al_2O_3 (Figs. 6, 8; Table 1). This implies that the cumulus association contained plagioclase and did not contain hornblende and may indicate that the sanukitoid melts may have contained relatively low H_2O concentrations (Stern et al., 1989).

The granodiorites and tonalites of the Shuya Massif show many compositional features analogous to those of the sanukitoids of the Hautavaara Massif (which bear similar SiO_2 concentrations) but differ from them in having lower concentrations of HFSE and REE and lower $\varepsilon_{Nd}(T) = –2.8$, which indicates that that melt sources were different. The low-radiogenic Nd isotopic composition and the presence of ancient inherited zircon indicate that the granodiorites of the Shuya Massif were derived by the melting of an ancient crustal source: $T_{Nd}(DM) = 3.25$ Ga (Table 3). The aforementioned blue color of quartz in the granodiorites of the Shuya Complex may be explained by that the quartz contains minute rutile inclusions because the magmatic quartz was originally rich in TiO_2 (Savko et al., 2019). This, in turn, may imply that the granodiorite melt has a high temperature (Wark and Watson, 2006), which could be caused in the crust by coeval mafic sanukitoid melts. A probable contribution of mafic sanukitoid melts to the petrogenesis of the granodiorites of the Shuya Massif also follows from that the rocks contain elevated Ni and Cr concentrations (Table 1, Fig. 7).

The leucogranites of the Nyalmozero Massif exhibit contrastingly different geochemical and isotopic features and obviously belong to another genetic group of granitoids. The negative $\varepsilon_{Nd}(T) = –0.9$ indicates a crustal source of the melt, which had a long-

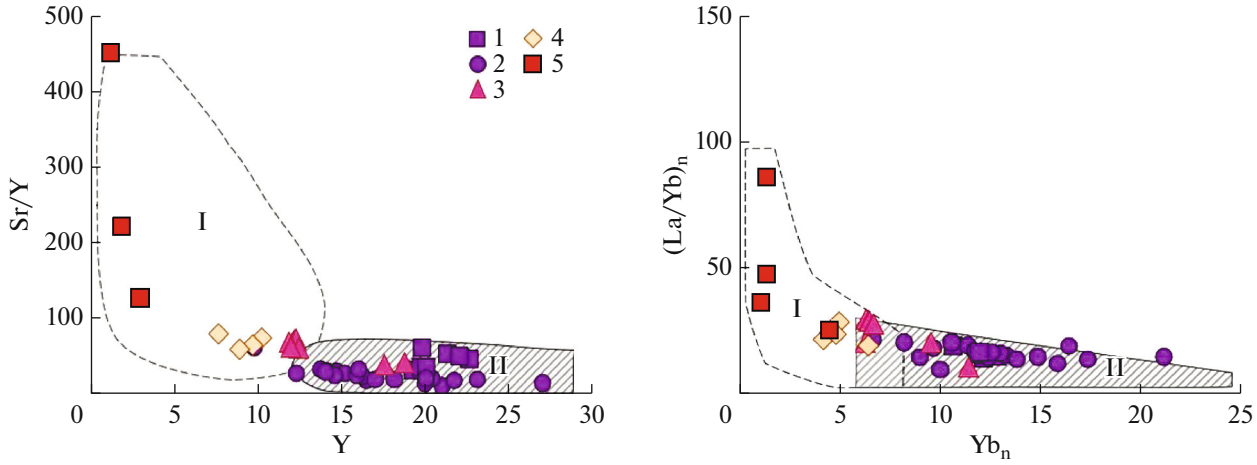

Fig. 12. Sr/Y–Y and $(La/Yb)_n$–Yb_n diagrams for granitoids of the Hautavaara Structure. Massifs: (1, 2) Hautavaara ((1) phase 1, (2) phase 2); (3) Chalka; (4) Shuya; (5) Nyalmozero. Composition fields: (I) adakite, (II) calc-alkaline island-arc series (Zhang et al., 2019).

lasting prehistory: $T_{Nd}(DM) = 3.06$ Ga (Table 3). The very low HREE concentrations and the strongly fractionated patterns of these elements mean that the leucogranitic melts were formed in equilibrium with a garnet-bearing residue, which suggests that the melt was derived at depths greater than 15–20 km (Gao et al., 2016). Granites with similar characteristics are also known to occur in the Vedlozero–Segozero Belt in close association with the sanukitoids of the Bergaul Massif (Larionova et al., 2007).

The territory of the Hautavaara Structure was thus simultaneously, at approximately 2.74 Ma, intruded by acid melts derived from different lithospheric sources, including the metasomatized mantle and different crustal levels.

Sources and Tectonic Environment of the Derivation of the Granitoid Melts of the Hautavaara Structure

Petrogenetic models with the derivation of the parental melts of sanukitoids by means of melting mantle sources imply that the environments in which these melts are derived were close to island-arc environments, whose magmatism is related to suprasubductional metasomatic recycling and melting of the mantle wedge (Stevenson et al., 1999). This is clearly illustrated in the Sr/Y–Y and La/Yb–Yb diagrams: the composition points of the sanukitoids plot within the field of arc calc-alkaline volcanic rocks (Fig. 12).

The mineral composition and some petrochemical features of granitoids in the Hautavaara Structure are the closest to those of I-type granites (Fig. 13). Their A/CNK = 0.7–1.1. Sanukitoids of unusual composition sometimes show characteristics of different geochemical types of granitoids. The high HFSE (Zr, Y, and Nb) concentrations in granitoids of the Hautavaara Structure (Fig. 7) are a feature typical of A-type granites, but these rocks are rich in LILE (Ba and Sr), which is atypical of A-type granites. In the Pearce discriminant diagrams, the composition points of granitoids from the Hautavaara Structure plot mostly within the field of island-arc granites (Fig. 13).

The different tectonic setting of the sanukitoids and their different age from those of all Neoarchean GGP, including the Karelian GGP, provide grounds to believe that these rocks were formed in a post-subduction environment and that their mantle source was formed in relation to episodes of suprasubductional metasomatism, when TTG granitoids were produced (Samsonov et al., 2004; Kovalenko et al., 2005; Larionova et al., 2007; Lobach-Zhuchenko et al., 2008; Höltta et al., 2012). The evolution of the Hautavaara Structure and characteristics of granitoids in its surroundings are consistent with this tectonic model.

According to available data, the Vedlozero–Segozero Greenstone Belt was produced at 3.04–2.85 Ga in the course of accretion and subduction processes on a margin of the Vodlozero Domain of the continental crust. Data on structures in the belt indicate that its evolutionary history involved two major episodes (Svetov and Svetova, 2011; Svetov et al., 2006). The first of them occurred at 3.05–2.90 Ga and produced the basalt–andesite–dacite–rhyolite and komatiite–basalt volcanic associations, which may have been formed in the environment of an oceanic island arc and later accreted at the margin of the Vodlozero Domain. The ensimatic environment in which the rock associations of the first episode were formed, with a minor addition of ancient crustal material, is illustrated by the $\varepsilon_{Nd}(T)$–T diagram, in which all composition points of the magmatic rocks of this episode define an individual field outside the evolutionary trend of the

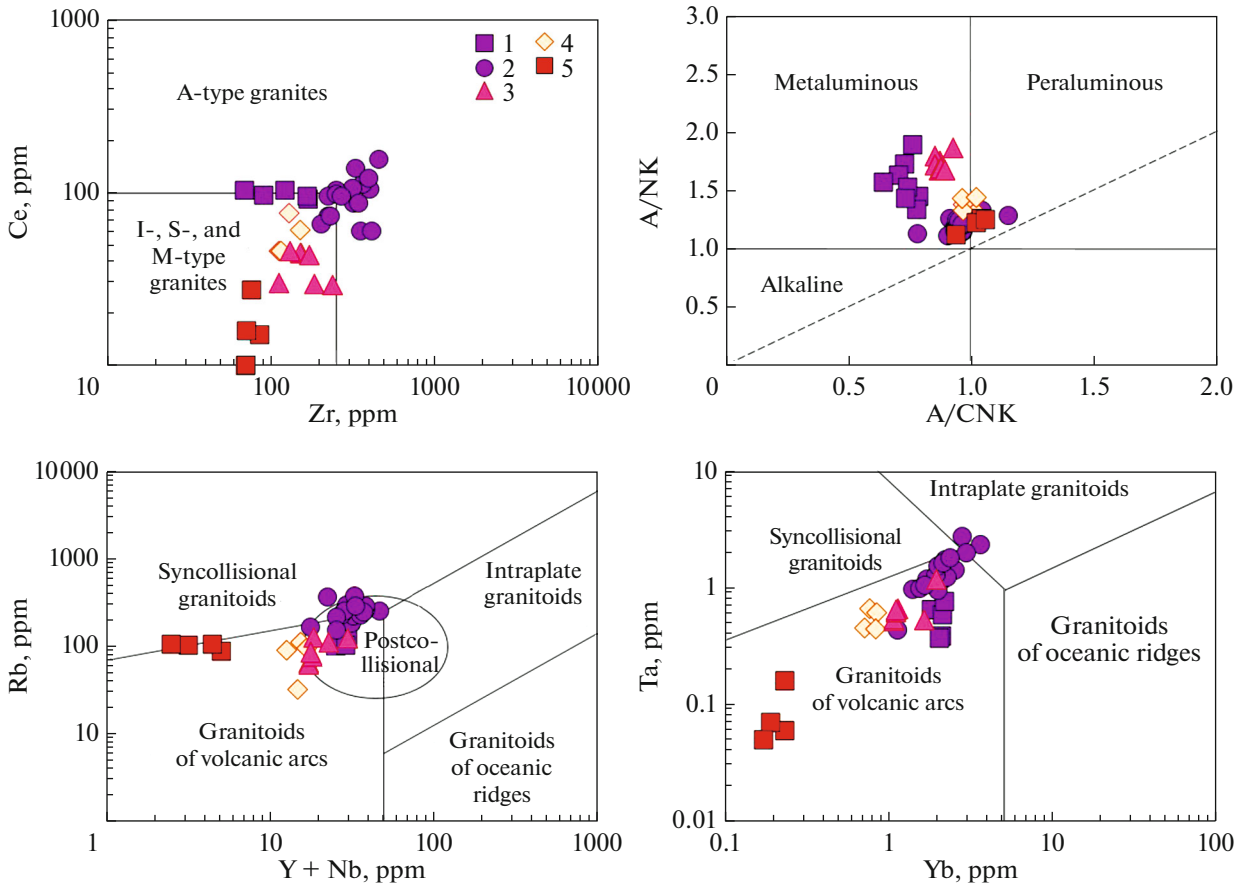

Fig. 13. Discriminant diagrams Ce–Zr (Whalen et al., 1987), A/NK–A/CNK (Maniar and Piccoli, 1989), and Rb–(Y + Nb) and Ta–Yb (Pearce, 1996) for granitoids of the Hautavaara Structure. Massifs: (1, 2) Hautavaara ((1) phase 1, (2) phase 2); (3) Chalka; (4) Shuya; (5) Nyalmozero.

Nd isotope composition of Paleoarchean TTG gneisses of the adjacent Vodlozero Domain (Fig. 14).

The second episode, at 2.90–2.85 Ga, has produced volcanics of the dacite–rhyolite association, which were formed in a continental-margin environment on a crust of heterogeneous age, which included the Paleoarchean TTG gneisses of the Vodlozero Domain and Mesoarchean arc complexes of the first episode. This tectonic environment was responsible for the derivation of volcanic rocks with very broad variations in the Nd initial isotope composition, up to sources with an Eoarchean crustal prehistory (Fig. 14).

The variations in the isotopic–geochemical characteristics of the 2.74-Ga granitoids seem to reflect the isotopic–geochemical heterogeneity of the lithosphere, which was formed by earlier Mesoarchean events of different age. The composition points of sanukitoids in the Hautavaara and Chalka massifs, as well as sanukitoids in other structures of the Vedlozero–Segozero Greenstone Belt, show a juvenile Nd isotope composition and were likely produced by the melting of a mantle source that had been metasomatized during the second evolutionary episode of the greenstone belt (Fig. 14). By contrast, the granodiorites of the Shuya Complex, leucogranites of the Nyalmozero Massif, and their analogues in the Bergaul Structure may have been formed by the melting of 3.05- to 2.90-Ga crust with isotope characteristics of the first, older association (Fig. 14).

The geodynamic reasons for the generation of granite magmas at 2.74 Ga are widely discussed in the literature. The separation of the granitoids with an age of 2.74 Ga from older magmatic episodes at 3.05–2.85 Ga in the Vedlozero–Segozero Belt rules out models involving slab breakoff and the opening of a slab window (Beakhouse and Davis, 2005). A more realistic model seems to be the collapse of the collisional orogen (Kusky, 1993; Laurent et al., 2014), with the melting of the metasomatized mantle beneath the whole Karelian Craton, including the Vedlozero–Segozero Belt, which was triggered by the ascent of a mantle diapir in response to the thinning of the lithosphere that had been overthickened by processes of gravitational and thermal relaxation.

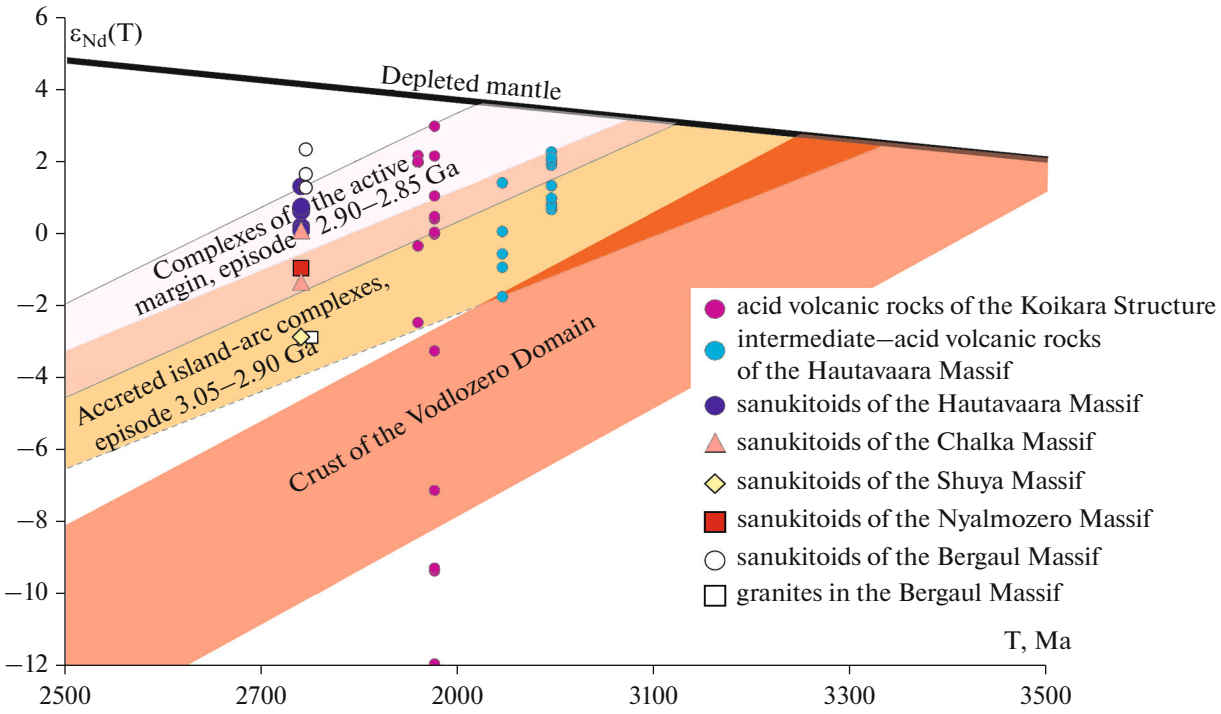

Fig. 14. $\varepsilon_{Nd}(T)$–T diagram for rocks of the Vodlozero Domain (Kulikov et al., 1990; Lobach-Zhuchenko et al., 2000; Puchtel et al., 2016), volcanic rocks of the Vedlozero–Segozero Greenstone Belt (based on data in Ovchinnikova et al., 1994; Samsonov et al., 1996; Svetov et al., 2006; Gogolev et al., 2018), post-tectonic granitoids of the Hautavaara Structure (Lobach-Zhuchenko et al., 2000; Kovalenko et al., 2005; this publication), and the Bergaul Massif (Larionova et al., 2007). See the text for discussion of the shaded fields corresponding to the evolution of the Nd isotope composition of rock complexes in the Vedlozero–Segozero Belt. The depleted mantle is according to (Goldstein and Jacobsen, 1988).

CONCLUSIONS

1. The post-tectonic granitoids of different composition, including sanukitoids, granodiorites, and leucogranites in the Hautavaara Structure, were emplaced within a narrow age range, likely within a single episode of magmatic activity.

2. The difference in the complex of the granitoids were formed due to a number of reasons, including the melting of compositionally diverse mantle (for the sanukitoids) and crustal (for the granitoids) sources, crystallization differentiation of the sanukitoid melts, and mixing of the sanukitoid and granite magmas.

3. The simultaneous melting of lithosphere at different depth levels was triggered by the ascent of an asthenospheric diapir, which was, in turn, associated with the collapse of the collisional orogen at about 2.7 Ga, during the final episode of the tectonic evolution of the Karelian GGP, with crust-forming processes in it occurring in the environment of a convergent plate boundary.

ACKNOWLEDGMENTS

The authors thank Corresponding Member of the Russian Academy of Sciences A.V. Samsonov for the careful review of the manuscript and for valuable comments expressed in the course of the discussions. The authors thank A.V. Stepanova for continuing assistance and aid when this research was carried out. A.V. Karvinen is thanked for preparing the samples. We also thank the staff of the Analytical Center at the Institute of Geology, Karelian Research Centre, Russian Academy of Sciences.

FUNDING

This study was carried out under government-financed research project AAAA-A18-118020290084-7 for the Institute of Geology, Karelian Research Centre, Russian Academy of Sciences, and was financially supported by the Russian Foundation for Basic Research, project no. 18-35-00447.

REFERENCES

Arestova, N.A., Chekulaev, V.P., Lobach-Zhuchenko, S.B., and Kucherovskii, G.A., Formation of the Archean Crust of the Ancient Vodlozero Domain (Baltic Shield), *Stratigraphy. Geol. Correlation,* 2015, vol. 23, no. 2, pp. 119–130.

Beakhouse, G.P. and Davis, D.W., Evolution and tectonic significance of intermediate to felsic plutonism associated with the Helmo greenstone belt, Superior Provimce, Canada, *Precambrian Res.,* 2005, vol. 137, pp. 61–92.

Bibikova, E.V., Samsonov, A.V., Shchipanskii, A.A., et al., The Hisovaara Structure in the Northern Karelian Greenstone Belt as a Late Archean accreted island arc: isotopic geochronological and petrological evidence, *Petrology,* 2003, vol. 11, no. 3, pp. 261–290.

Bibikova, E.V., Petrova, A., and Claesson, S., The temporal evolution of the sanukitoids in the Karelian Craton, Baltic Shield: an ion microprobe U-Th-Pb isotopic study of zircons, *Lithos,* 2005, vol. 79, pp. 129–145.

Black, L.P., Kamo, S.L., Allen, C.M., et al., TEMORA 1: a new zircon standard for phanerozoic U-Pb geochronology, *Chem. Geol.*, 2003, vol. 200, pp. 155–170.

Chekulaev V.P. Archean "sanukitoids" on the Baltic Shield, *Dokl. Earth Sci.,* 1999, vol. 369, no. 8, pp. 1137–1139.

Chekulaev, V.P., Arestova, N.A., Egorova, Yu.S., and Kucherovskii, G.A., Change of conditions of the formation of the Karelian Province of the Baltic Shield continental crust during transition from Meso- to Neoarchean: geochemical study results, *Stratigraphy. Geol. Correlation,* 2018, vol. 26, no. 3, pp. 243–260.

Chekulaev, V.P., Arestova, N.A., and Egorova, Yu.S., Neoarchean granites of the Karelian Province: geological position, geochemistry, and origin, *Regional. Geol. Metallogen.,* 2020, vol. 81, pp. 21–38.

Condie, K.C., *Archean Greenstone Belts,* Amsterdam: Elsevier, 1981.

Dmitrieva, A.V., Kuleshevich, L.V., and Vikhko, A.S., Petrochemical features and ore specialization of the Khautovaara massif, Southern Karelia, *Tr. KarNTs RAS,* 2016, no. 2, pp. 52–70.

Gao, P., Zheng, Y.F., and Zhao, Z.F., Experimental melts from crustal rocks: a lithochemical constraint on granite petrogenesis, *Lithos,* 2016, vol. 266, pp. 133–157.

Gogolev, M.A., Geochemical typification of dacite–rhyolite magmatism of the central part of the Vedlozero–Segozero greenstone belt, Karelian Craton, *Tr. KarNTs RAS,* 2018, 11. S. 82-95.

Goldstein, S.J. and Jacobsen, S.B., Nd and Sm isotopic systematics of rivers water suspended material: implications for crustal evolution, *Earth Planet. Sci. Lett.,* 1988, vol. 87, pp. 249–265.

Halla, J., Late Archean high-Mg granitoids (sanukitoids) in the southern Karelian domain, eastern finland: pb and nd isotopic constraints on crust-mantle interactions, *Lithos,* 2005, vol. 79, pp. 161–178.

Heilimo, E., Halla, J., and Huhma, H., Single-grain zircon U-Pb age constraints of the western and eastern sanukitoid zones in the Finnish part of the Karelian Province, *Lithos,* 2011, vol. 121, pp. 87–99.

Höltta, P., Heilimo, E., Huhma, H., et al., The Archaean of the Karelia province in Finland, *Geol. Surv. Finland. Spec. Paper,* 2012, no. 54, pp. 21–73.

Jacobsen, S.B. and Wasserburg, G.J., Sm-Nd evolution of chondrites and achondrites, *Earth Planet. Sci. Lett.,* 1984, vol. 67, pp. 137–150.

Kotov, A.B., Kovach V.P., Salnikova, E.B., et al., Age and formation stages of continental crust of the central Aldan granulite terrane: U-Pb and Sm-Nd isotope data on granitoids, *Petrologiya,* 1995. vol. 3, no. 1, pp. 97–108.

Kovalenko, A.V., Clemens, J.D., and Savatenkov, V.M., Petrogenetic constraints for the genesis of Archaean sanukitoid suites: geochemistry and isotopic evidence from Karelia, Baltic Shield, *Lithos,* 2005, vol. 79, pp. 147–160.

Kozhevnikov V.N. *Arkheiskie zelenokamennye poyasa Karel'skogo kratona kak akkretsionnye orogeny* (Archean Greenstone Belts of the Karelian Craton as Accretionary Orogens), Petrozavodsk: IG KarNTs RAS, 2000.

Kuleshevich, L.V., Slyusarev, V.D., and Lavrov, M.M., Noble metal mineralization of the Khautavaara–Vedlozero area, *Geol. Polezn. Iskop. Karelii,* 2009, vol. 12, pp. 12–25.

Kulikov, V.S., Simon, A.K., Kulikova, V.V., et al., *Magmatic evolution of the Vodlozero block of the Karelian granite–greenstone terrane in the Archean, Geologiya i geokhronologiya dokembriya Vostochno-Evropeiskoi platform (Precambrian Geology and Geochronology of the East European Platform)*, Leningrad: Nauka, 1990, pp. 92–100.

Kusky, T.M., Collapse of Archaen orogens and the generation of late- to postkinematic granitoids, *Geology,* 1993, vol. 21, pp. 925–928.

Larionov, A.N., Andreichev, V.A. and Gee, D., The Vendian alkaline igneous suite of northern Timan: ion microprobe U-Pb zircon ages of gabbros and syenite, *Geol. Soc., London, Spec. Publ.,* 2004, pp. 69–74.

Larionova, Yu.O., Samsonov, A.V., and Shatagin, K.N., Sources of Archean sanukitoids (high-Mg subalkaline granitoids) in the Karelian Craton: Sm-Nd and Rb-Sr isotopic-geochemical evidence, *Petrology,* 2007, vol. 15, no. 6, pp. 530–550.

Laurent, O., Martin, H., Moyen, J.F., and Doucelance, R., The diversity and evolution of Late-Archean granitoids: evidence for the onset of "modern-style" plate tectonics between 3.0 and 2.5 Ga, *Lithos,* 2014, vol. 205, pp. 208–235.

Lobach-Zhuchenko, S.B., Chekulaev, V.P., Arestova, N.A., et al., *Archean Terranes in Karelia: Geological and Isotopic–Geochemical Evidence, Geotectonics*, 2000, vol. 34, no. 6, pp. 452–466.

Lobach-Zhuchenko, S.B., Chekulaev, V.P., Ivanikov, V.V., et al., *Late Archean high-Mg and subalkaline granitoids and lamprophyres as indicator of gold mineralization in Karelia (Baltic Shield), Russia, Ore-Bearing Granites of Russia and Adjacent Countries,* Moscow: IMGRE, 2000, pp. 193–211.

Lobach-Zhuchenko, S.B., Rollinson, H.R., Chekulaev, V.P., et al., The Archaean sanukitoid series of the Baltic Shield: geological setting, geochemical characteristics and implications for their origin, *Lithos,* 2005, vol. 79, pp. 107–128.

Lobach-Zhuchenko, S.B., Rollinson, H., Chekulaev, V.P., et al., Petrology of a Late Archaean, highly potassic, sanukitoid pluton from the Baltic Shield: insights into Late Archaean mantle metasomatism, *J. Petrol.,* 2008, vol. 49, pp. 393–420.

Ludwig, K.R., *SQUID. A User's manual*, *Berkeley Geochronol. Center, Spec. Publ.,* 2001.

Ludwig, K.R., *User's manual for ISOPLOT 3.00. Geochronological toolkit for Microsoft Excel*, *Berkeley Geochronol. Center. Spec. Publ.,* 2003.

Maniar, P.D. and Piccoli, P.M., Tectonic discrimination of granitoids, *Geol. Soc. Am. Bull.,* 1989, vol. 101, pp. 635–643.

Martin, H., Moyen, J.-F., and Rapp, R.P., The sanukitoid series: magmatism at the Archaean–Proterozoic transition, *Earth Environ. Sci. Trans. R. Soc. Edinburgh,* 2009, vol. 100, pp. 15–33.

Matrenichev, V.A., Sergeev, S.A., Levchenkov, O.D., and Yakovleva, S.Z., Age of dacites of the Khautavaara greenstone structure, Central Karelia, Izv. Aakad. Nauk, Ser. Geol., 1990, no. 8, pp. 131–133.

Mikkola, P., Salminen, P., Torppa, A., and Huhma, H., The 2.74 Ga Likamännikkö complex in uomussalmi, East Finland: lost between sanukitoids and truly alkaline rocks?, *Lithos,* 2011, vol. 1050, no. 125, pp. 716–728.

Nosova, A.A., Samsonov, A.V., Larionova, Yu.O., et al., Archean age of gabbro and granite—biotite—amphibole—quartz metasomatites of the Vietukkalampi Au-PGE occurrence in the Khautavaara structure, *Sb. materialov Mezhdunarodnoi konf. "Zoloto Fennoskandinavskogo shchita"* (Proc. International Conference "Gold of the Fennoscandian Shield), Petrozavodsk: IG KarNTs RAS, 2013, pp. 131–134.

Ovchinnikova, G.V., Matrenichev, V.A., Levchenkov, O.A., et al., U-Pb and Pb-Pb isotopic studies of acid volcanic rocks of the Khautavaara greenstone structure, Central Kaelia, *Petrologiya,* 1994, vol. 2, no. 3, pp. 266–281.

Pearce, J.A., Sources and settings of granitic rocks, *Episodes,* 1996, vol. 19, no. 4, pp. 120–125.

Puchtel, I.S., Hofmann, A.W., Jochum, K.P., et al., The Kostomuksha greenstone belt, N.W. Baltic Shield: remnant of a Late Archean oceanic plateau?, *Terra Nova,* 1997, vol. 9, pp. 87–90.

Puchtel, I.S., Hofmann, A.W., Amelin, Yu.V., et al., Combined mantle plume–island arc model for the formation of the 2.9 Ga Sumozero–Kenozero greenstone belt, SE Baltic Shield: isotope and trace element constraints, *Geochim. Cosmochim. Acta,* 1999, vol. 63, no. 21, pp. 3579–3595.

Puchtel, I.S., Touboul, M., Blichert-Toft, J., et al., Lithophile and siderophile element systematics of Earth's mantle at the Archean–Proterozoic boundary: evidence from 2.4 Ga komatiites, *Geochim. Cosmochim. Acta,* 2016, vol. 180, pp. 227–255.

Rannii dokembrii Baltiiskogo shchita (Early Precambrian of the Baltic Shield), Glebovitskii, V.A., Eds., St. Petersburg: Nauka, 2005.

Rapp, R.P., Shimizu, N., Norman, M.D., and Applegate, G.S., Reaction between slab-derived melts and peridotite in the mantle wedge: experimental constraints at 3.8 GPa, *Chem. Geol.,* 1999, vol. 160, pp. 335–356.

Rapp, R., Norman, M., Laporte, D., et al., Continent formation in the Archean and chemical evolution of the cratonic lithosphere: melt-rock reaction experiments at 3–4 GPa and petrogenesis of Archean Mg-diorites (sanukitoids), *J. Petrol.,* 2010, vol. 51, pp. 1237–1266.

Rybakov, S.I., Svetova, A.I., Kulikov, V.S., et al., *Vulkanizm arkheiskikh zelenokamennykh poyasov Karelii* (Volcanism of Archean Greenstone Belts of Karelia), Leningrad: Nauka, 1981.

Rybakov, S.I., Grishin, A.S., Kozhevnikov, V.N., et al. *Metallogenicheskaya evolyutsiya arkheiskikh zelenokamennykh poyasov Karelii. Ch. 1. Vulkanizm, sedimentogenez, metamorfizm i metallogeniya* (Metallogenic Evolution of Archean Greenstone Belts of Karelia. Part 1. Volcanism, Sedimetogenesis, Metamorphism, and Metallogeny), St. Petersburg: Nauka, 1993.

Samsonov, A.V., Bibikova, E.V., and Puchtel, I.S., et al., Isotope and geochemical variations of the acid volcanics of the karelian greenstone belts and their geotectonic significance, *Abstracts for the First International Symposium "Fennoscandian Geological Correlation,"* St. Petersburg, 1996.

Samsonov, A.V., Bibikova, E.V., Larionova, Yu.O., et al., Magnesian granitoids (sanukitoids) of the Kostomuksha area, Western Karelia: petrology, geochronology, and tectonic environment of formation, *Petrology*, 2004, vol. 12, no. 5, pp. 437–468.

Savko, K.A., Samsonov, A.V., Larionov, A.N., et al., 2.6 Ga high-Si rhyolites and granites in the Kursk domain, eastern Sarmatia: petrology and application for the Archaean palaeocontinental correlations, *Precambrian Res.,* 2019, vol. 322, pp. 170–192.

Sharpenok, L.N., Kostin, A.E., and Kukharenko, E.A., TAS-diagram total alkalis–silica for the chemical classification and diagnostics of plutonic rocks, *Regional. Geol. Metallogen.,* 2013, vol. 56, pp. 40–50.

Slyusarev, V.D., Kuleshevich, L.V., and Lavrov, M.M., Noble metal mineralization in the gabbroid massif of the Lake Vietukkalampi area, Khautavaara structure, Mineralogiya, petrologiya i minerageniya dokembriiskikh kompleksov Karelii (Mineralogy, Petrology, and Metallogeny of the Precambrian Complexes of Karelia), Petrozavodsk: IG KarNTs RAS, 2007, pp. 112–116.

Stepanova, A.V., Samsonov, A.V., Salnikova, E.B., et al., Paleoproterozoic continental MORB-type tholeiites in the Karelian craton: petrology, geochronology and tectonic setting, *J. Petrol.,* 2014, vol. 55, no. 9, pp. 1719–1751.

Stern, R.A., Hanson, G.N., and Shirey, S.B., Petrogenesis of mantle-derived, LILE-enriched archean monzodiorites and trachyandesites (sanukitoids) in southwestern superior province, *Can. J. Earth Sci.,* 1989, vol. 26, pp. 1688–1712.

Stern, R.A. and Hanson, G.N., Archaean high-mg granodiorite: a derivative of light rare earth element-enriched monzodiorite of mantle origin, *J. Petrol.,* 1991, vol. 32, no. 1, pp. 201–238.

Stevenson, R., Henry, P., and Gariepy, C., Assimilation–fractional crystallization origin of Archaean sanukitoid suites: Western Superior Province, Canada, *Precambrian Res.,* 1999, vol. 96, pp. 83–99.

Sun, S.-S. and McDonough, W.F., Chemical and isotopic systematics of oceanic basalts: implications for mantle composition and processes, *Geol. Soc. London. Spec. Publ.,* 1989, no. 42, pp. 313–345.

Svetov, S.A., *Magmaticheskie sistemy zon perekhoda okean-kontinent v arkhee vostochnoi chasti Fennoskandinavskogo shchita* (Archean Magmaic Systems of the Ocean–Continent Transition Zones in the Fennoscandian Shield), Petrozavodsk: IG KarNTs RAS, 2005.

Svetov, S.A. and Huhma, H., Geochemistry and Sm–Nd systematics of the Archean komatiitic–tholeiitic associations of the Vedlozero–Segozero greenstone belt, Central Karelia, *Dokl. Earth Sci.,* 1999, vol. 369, no. 9, pp. 1204–1206.

Svetov, S.A., Kudryashov, N.M., Ronkin, Yu.L., Huhma, H., Svetova, A.I., and Nazarova, T.N., Mesoarchean island-arc association in the Central Karelian Terrane, Fennoscandian Shield: new geochronological data, *Dokl. Earth Sci.,* 2006, vol. 406, no. 1, pp. 103–106.

Svetov, S.A., Stepanova, A.V., Chazhengina, S.Yu., et al., Precision (ICP-MS, LA-ICP-MS) analysis of rock and mineral composition: technique and assessment of result

accuracy by the example of the Early Precambrian mafic complexes, *Tr. KarNTs RAS,* 2015, no. 7, pp. 54–73.

Svetov, S.A. and Svetova, A.I., Archean subduction: marker rock associations and architecture, *Materialy Vseros. konf. "Geologiya Karelii ot arkheya do nashikh dnei"* (Proc. All-Russian Conference "Geology of Karelia from Archean to the Present Day"), Petrozavodsk: IG KarNTs RAS, 2011, pp. 22–32.

Wark, D.A. and Watson, E.B., TitaniQ: a titanium-in-quartz geothermometer, *Contrib. Mineral. Petrol.,* 2006, vol. 152, pp. 743–754.

Whalen, J.B., Currie, K.L., and Chappell, B.W., A-type granites: geochemical characteristics, discrimination and petrogenesis, *Contrib. Mineral. Petrol.,* 1987, vol. 95, pp. 407–419.

Wiendenbeck, M., Alle, P., Corfu, F., et al., Three natural zircon standards for U-Th-Pb, Lu-Hf, trace element and REE analyses, *Geostand. Newslett.,* 1995, vol. 19, pp. 1–23.

Williams, I.S., Applications of microanalytical techniques to understanding mineralizing processes, *Rev. Econ. Geol.,* 1998, vol. 7, pp. 1–35.

Zhang, L., Li, S., and Zhao, Q., A review of research on adakites, *Int. Geol. Rev.,* 2019, vol. 63, pp. 1–18.

Translated by E. Kurdyukov